# Magnetic Topology in Coupled Binaries, Spin-orbital Resonances, and Flares

Sergey A. Cherkis<sup>1</sup> and Maxim Lyutikov<sup>2</sup>

#### Abstract

We consider topological configurations of the magnetically coupled spinning stellar binaries (e.g., merging neutron stars or interacting star-planet systems). We discuss conditions when the stellar spins and the orbital motion nearly "compensate" each other, leading to very *slow* overall winding of the coupled magnetic fields; slowly winding configurations allow gradual accumulation of magnetic energy, which is eventually released in a flare when the instability threshold is reached. We find that this slow winding can be global and/or local. We describe the topology of the relevant space  $\mathbb{F} = T^l S^2$  as the unit tangent bundle of the two-sphere and find conditions for slowly winding configurations in terms of magnetic moments, spins, and orbital momentum. These conditions become ambiguous near the topological bifurcation points; in certain cases, they also depend on the relative phases of the spin and orbital motions. In the case of merging magnetized neutron stars, if one of the stars is a millisecond pulsar, spinning at  $\sim 10$  ms, the global resonance  $\omega_1 + \omega_2 = 2\Omega$  (spin-plus beat is two times the orbital period) occurs approximately one second before the merger; the total energy of the flare can be as large as 10% of the total magnetic energy, producing bursts of luminosity  $\sim 10^{44}$  erg s<sup>-1</sup>. Higher order local resonances may have similar powers, since the amount of involved magnetic flux tubes may be comparable to the total connected flux.

Unified Astronomy Thesaurus concepts: Interacting binary stars (801); Neutron stars (1108)

#### 1. Introduction

Direct magnetospheric interaction occurs in binary main-sequence stars (e.g., epsilon Lupi system, Shultz et al. 2015), white dwarf binaries (Warner 1983; Buckley et al. 2017), planetary systems (Rubenstein & Schaefer 2000; Antoine 2021), and has been suggested to occur between merging neutron stars (Hansen & Lyutikov 2001; Lyutikov 2011; Palenzuela et al. 2013; Radice et al. 2018; Lyutikov 2019; Most & Philippov 2020). In the latter case, it may lead to the precursor emission: production of an electromagnetic signal before the merger.

In the case of merging neutron stars, it is expected that the *persistent* power of the EM precursor is not very high, and not likely to be detected by all-sky high-energy monitors (Hansen & Lyutikov 2001; Lyutikov 2019; Most & Philippov 2020, and Section 5). Can the merging neutron stars produce flares that temporarily result in higher fluxes? Stellar flares that release up to 10<sup>7</sup> times more energy than the largest solar flare have been detected from main-sequence stars that host large planets (e.g., Schaefer et al. 2000). Rubenstein & Schaefer (2000) proposed that super-flares are caused by magnetic reconnection between the primary star and close-in Jovian planets. Following this ideas, we will investigate possible appearance of flares in magnetically interacting stars, and neutron stars in particular.

A magnetosphere of magnetically interacting stars is expected to have three types of regions (Figure 1), formed by magnetic field lines that (i) start and end on the same star, (ii) provide magnetic coupling, and (iii) connect to infinity (such regions appear both due to the spin of each star and orbital motion (Goldreich & Julian 1969); we ignore them here). The common part of the magnetosphere (magnetically coupled region ii) is twisted both by the relative spins of each companion, and by the orbital motion of the companions. Of particular interest are quasi-stationary configurations of the interacting magnetospheres, when the twisting produced by the orbital rotation is (partially) compensated by the spin(s) of the

binary. In such cases, we expect that the common magnetosphere is slowly wound/twisted by the combined effects of the components' spin and orbital motion; as a result, a fraction of the rotational energy is slowly stored in the magnetic field. After a system reaches some instability threshold, the stored magnetic energy can be released in (possibly) observable flares. In contrast, in highly time-dependent configurations, the energy release is expected to be nearly continuous. This results in smaller instantaneous luminosities and, in addition, quasisteady sources are harder to detect observationally.

In this paper, we discuss the topology of magnetically interacting stars and identify (quasi-) steady configurations, both global (when the whole magnetosphere returns to an initial state), and local (when only tubular neighborhoods of special magnetic field lines are untwisting).

The plan of the paper is as follows. In Section 2, we discuss qualitatively magnetic tube winding rate using the principle of braiding of present and future field lines. In Section 3, we discuss globally untwisting configurations. In Section 4, we develop a mathematical description of field line windings and use it to identify various possible resonances. In Section 5, we discuss astrophysical applications of the model.

# 2. The Concept of Magnetic Tube Winding

Consider two stars orbiting each other with orbital frequency  $\Omega$ . Consider distances much smaller than the (effective) light cylinder radius, so that, in the frame of the rotating stars, the effects of line sweep-back are not important. It is expected that, in all astrophysically important applications, the surrounding can be described as plasma: even in the case of merging neutron stars, when there is little external plasma, the magnetospheres are filled with self-generated electron-positron plasma (Goldreich & Julian 1969).

We are facing a complicated, time-dependent, three-dimensional, MHD problem (relativistic MHD in the case of merging

<sup>&</sup>lt;sup>1</sup> School of Mathematics, Institute for Advanced Study, Princeton NJ 08540, USA and Department of Mathematics, University of Arizona, 617 Santa Rita Avenue, Tucson AZ 85721-0089, USA; cherkis@ias.edu

Department of Physics and Astronomy, Purdue University, 525 Northwestern Avenue, West Lafayette, IN 47907-2036, USA; lyutikov@purdue.edu Received 2021 July 22; revised 2021 September 21; accepted 2021 September 22; published 2021 December 7

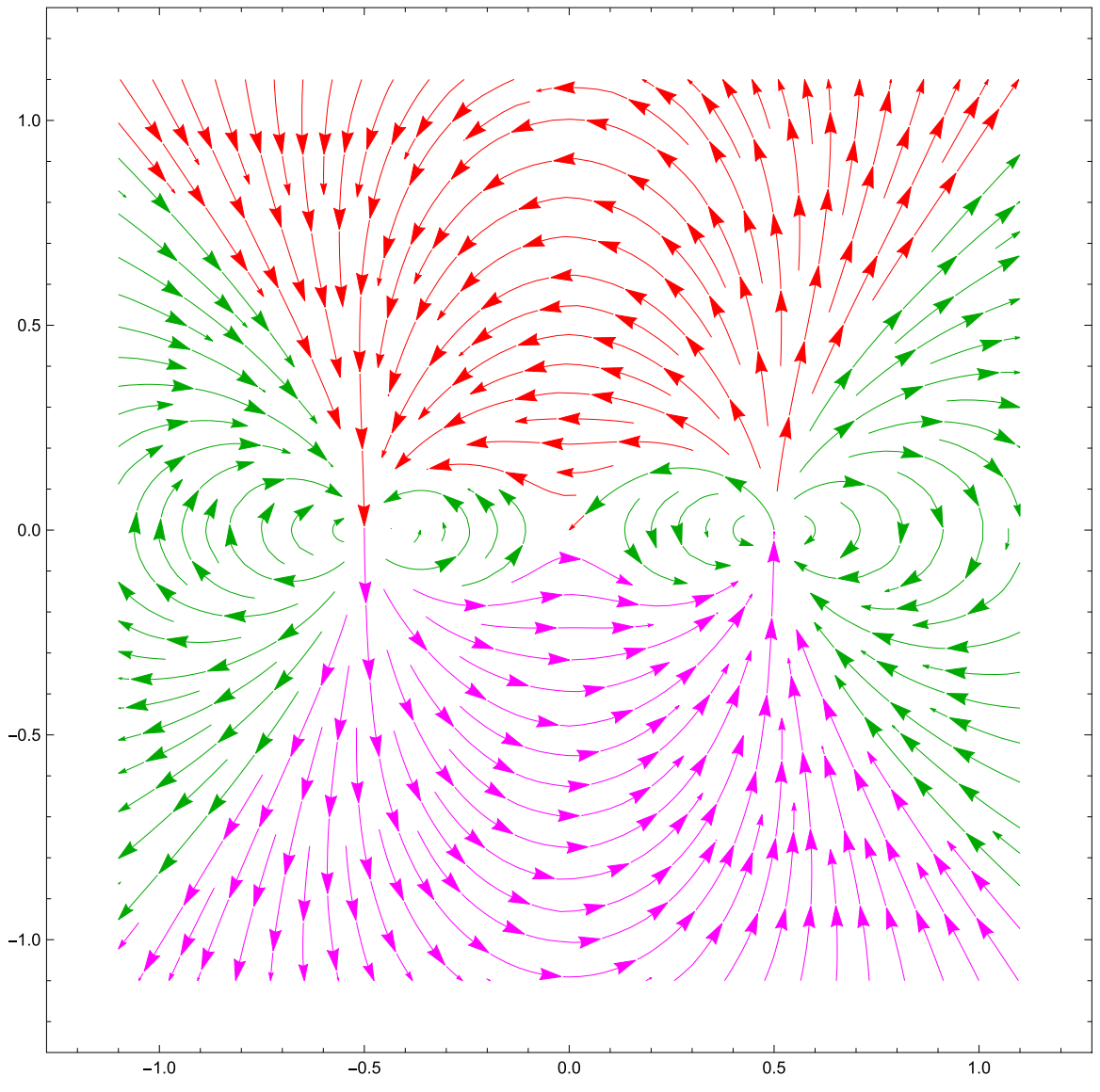


Figure 1. Example of magnetically coupled stars. The stars are located at  $x = \pm 0.5$  and have oppositely directed magnetic moments. The green field lines end on the same star from which they originate and form region (i). The red and magenta lines form region (ii), with red lines connecting the right star to the left one and the magenta lines connecting the left star to the right one.

neutron stars). To get a physical insight, let us think in terms of magnetic flux tubes; in nearly ideal plasma a magnetic flux tube has a clear physical interpretation due to the frozen-in condition. Let us next construct a physical model of the magnetic fields frozen in plasma, representing them as material objects: flux tubes. Each flux tube consists of nearby magnetic lines bundled together, forming a tubular neighborhood of its central line.

We are not interested in the twisting of each field line by itself (which is curl **B**), but rather we are interested in the rate at which a magnetic tube's twist increases (its winding rate). That means comparing how adjacent field lines and their images at a later time intertwine/braid around each other. Each field line can carry a current (can be twisted); this is not important. What we are after is the change in winding as measured by braiding of past and future magnetic lines. For example, each hair in a braid can be twisted on its own, but the topology of a braid is determined by how adjacent hairs interweave around it relative to each other. Clearly, it takes *three* strands to define a braid

(indeed, the hair braid needs at least three strands of hair). In our case, one of the strands will be the central line, another, the nearby line from the past, and the third, that same nearby line from the future. In more detail: since we are interested in the change of twisting of the flux tubes, it suffices to track its central line and one of the nearby lines (as a reference). This pair of lines can be thought of as a ribbon, with differently colored sides. Say, the central line is blue and its nearby line at the initial moment is red. Whenever, at some later moment, the central line happens to be sufficiently close to its original shape, we have the nearby line at that moment provide the third strand we need. Color the nearby line at that later moment green. Thus the braid consists of the blue central line strand (initial same as final), the red initial nearby line strand, and the green final nearby line strand. Then, at that moment, we can measure the winding of the final (green) nearby line around the (blue) central line relative to the (red) initial nearby line. The winding rate is that winding angle divided by the time increment.

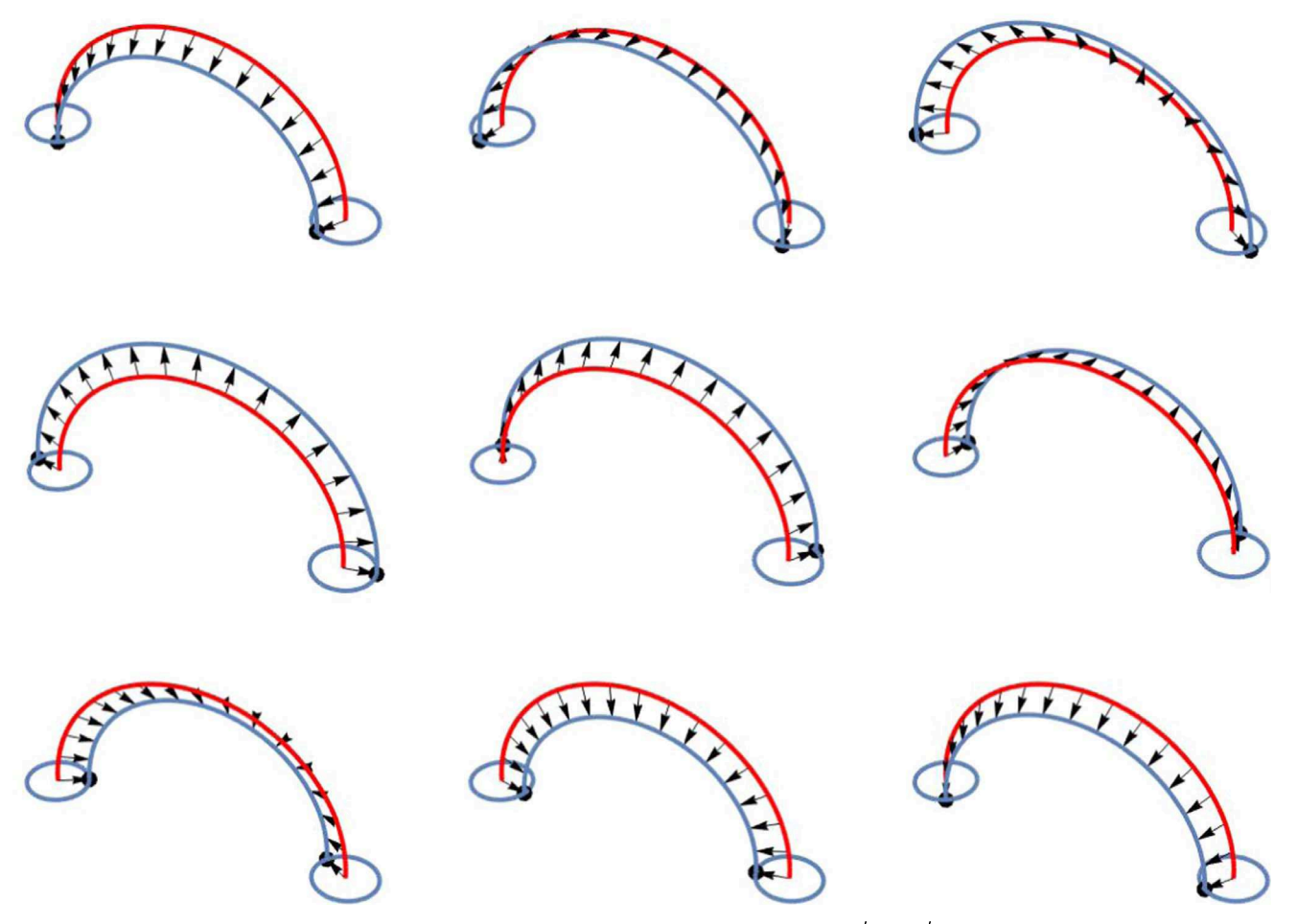


Figure 2. Basic configuration for Case II magnetically couples neutron stars in the corotating frame, where  $\omega_1' = -\omega_2'$ . The two neutron stars are represented by two disks connected by magnetic fields. Since we are not interested in the detailed dynamics here, but only in topological properties, we can approximate magnetic field lines as semicircles attached to particular points on the disks. Arrows indicate the normal field. After a full rotation, the system comes to the original state. Dots on the edges of the disks and differently colored flux lines help visually trace the evolution.

Of course, whenever the central line has no inflection points and, therefore, has a Frenet triad (consisting of a unit tangent, a principal normal, and their vector product), then there is a good notion of twisting: in this case, the twisting of the magnetic tube is the angle by which a nearby line winds relative to the principal normal as we traverse the line. This is usually called twisting and denoted by Tw (Moffatt & Dormy 2019). What we study is the rate of change in twisting  $\frac{d}{dt}Tw$ , which we call *winding rate*. This rate is well defined even when Tw is not (when the curve develops inflection points), as described above.

Intuitively, one might expect a relation of the above notion of magnetic tube twisting and helicity, since helicity measures average magnetic field self-linking (Arnold 1986, 1974). Indeed, there is some relation, though not as direct as one would like; namely, helicity is a sum of writhe and twist (Moffatt & Dormy 2019, Section 2.10). Our focus is on twist of the magnetic line, or, rather, on its rate of change. Thus our approach cannot be reduced to the commonly discussed magnetic helicity.

# 3. Globally Non-winding Magnetic Configurations of Orbiting Stars

#### 3.1. The Basic 2:1 Resonance

As discussed above, the key point to production of observable flares is the establishment of quasi-steady magnetic configuration, whereby the magnetic energy is slowly stored in the magnetospheres and later released in a sudden flare.

There are several basic cases where we expect that the whole interacting magnetospheres periodically return to their initial state. Consider first the case of magnetic moments parallel to the z-axis (one aligned, one counter-aligned, so that the two stars are magnetically connected) and spins also (anti)/parallel to z. Case I is a fully locked case:  $\omega_1 = \omega_2 = \Omega$ . In the rotating frame, this corresponds to  $\omega_1' = \omega_2' = 0$  (dashed quantities are measured in the corotating frame). Neutron stars are not expected to be tidally locked (Bildsten & Cutler 1992), so this case is unlikely to be realized and, consequently, is of no interest for us.

Case II is counter-aligned and spins in the corotating frame  $\omega_1' = -\omega_2'$  (and arbitrary  $\Omega$ ) (Figure 2). In this case, in the rotating frame, the configuration returns to the initial state. In the observer frame, this corresponds to the case when the frequency of beat-plus frequency equals two times the orbital frequency (Figures 3 and 4),

$$\omega_1 + \omega_2 = 2\Omega. \tag{1}$$

Importantly, the condition (1) applies to the beat-plus frequency  $\omega_1 + \omega_2$ , not each individual frequency separately. We call this 2:1 resonance: the sum of spins is two times the orbital frequency (Figure 3). This is the Dirac belt configuration. In the case of

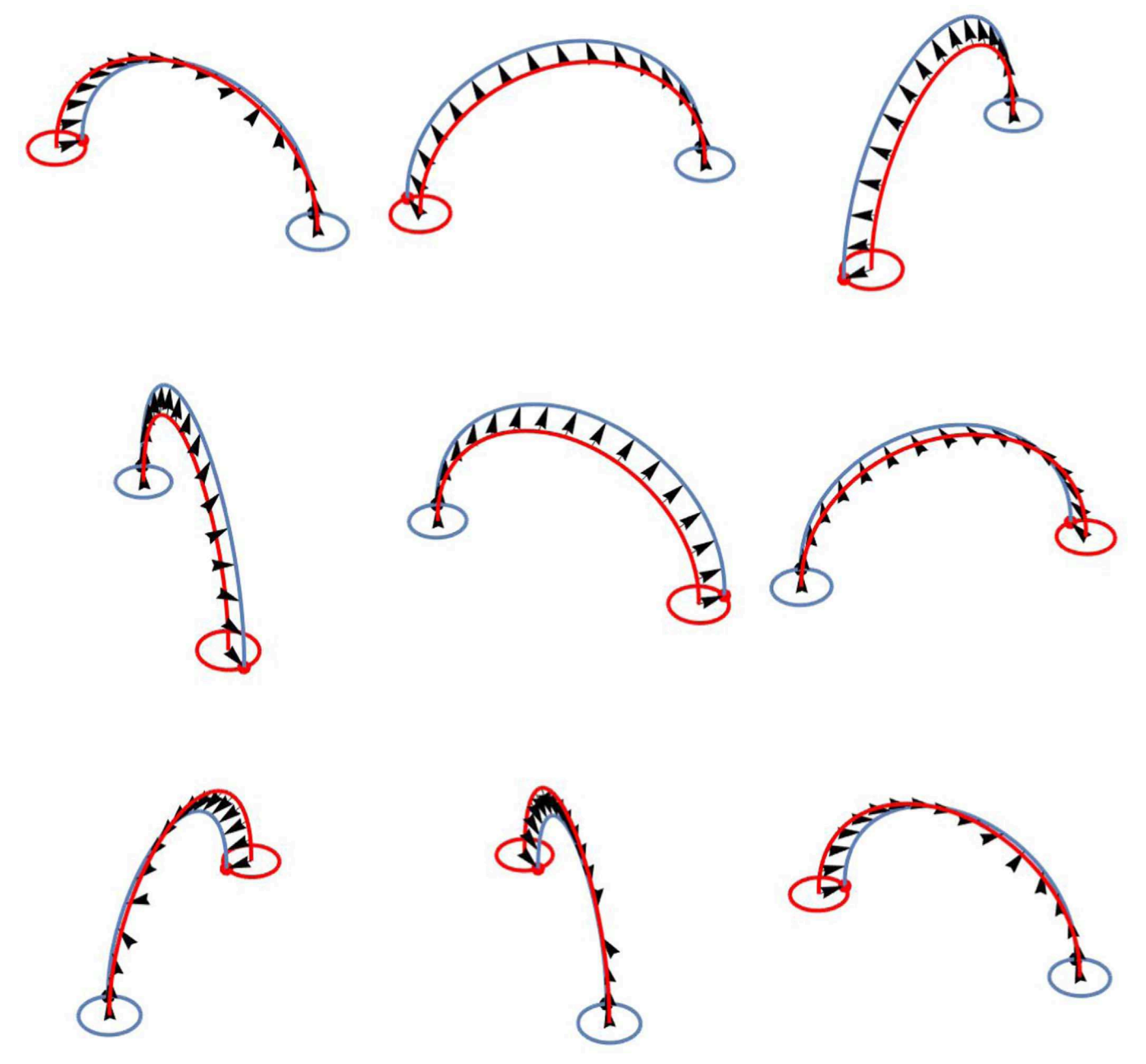


Figure 3. A basic example of the 2:1 spin-orbital resonance. In this example, the blue disk is non-rotating.

merging neutron stars, the changing orbital frequency may, at some point, become two times the sum of spins.

To the best of our knowledge, the 2:1 spin-orbital resonance has not been applied to magnetic fields of interacting binaries. In general physics, such a twisting arrangement is known under the names of "Dirac's belt" or "Feynman arrow" (also related to a "Plate trick").

#### 3.2. Variants of the 2:1 Resonance, Phases, and Bifurcations

In addition to the basic scenarios considered above, there are a number of more complicated cases. As we are about to demonstrate, the 2:1 resonance is more generic than the aligned case: it occurs for a wide variety of directions of spins and orbital axes and orientations of the intrinsic magnetic dipole moments. We shall now describe three indicative cases,

illustrating them in Figures 4–8 using table-top demonstrations. In the next section, we give a more economical description of the relevant geometry, and use it to revisit these illustrative cases again with better insight.

We number the two stars, let the first star not rotate at all, and, for definiteness, in all cases let the magnetic moments be counter-aligned along the z-axis at the initial moment (so that there is a strong magnetic coupling). Consider first when the spin of the second star is along the x-axis. Curiously, if the second star makes one spin rotation first, then half an orbit, then another full-spin rotation, and then another half an orbit, the configuration does not unwind (Figure 5). If, instead, the second star first makes two spin rotations, and then a full orbital rotation, the configuration does unwind (Figure 6). This example illustrates that the significance of the relative phase and angles.

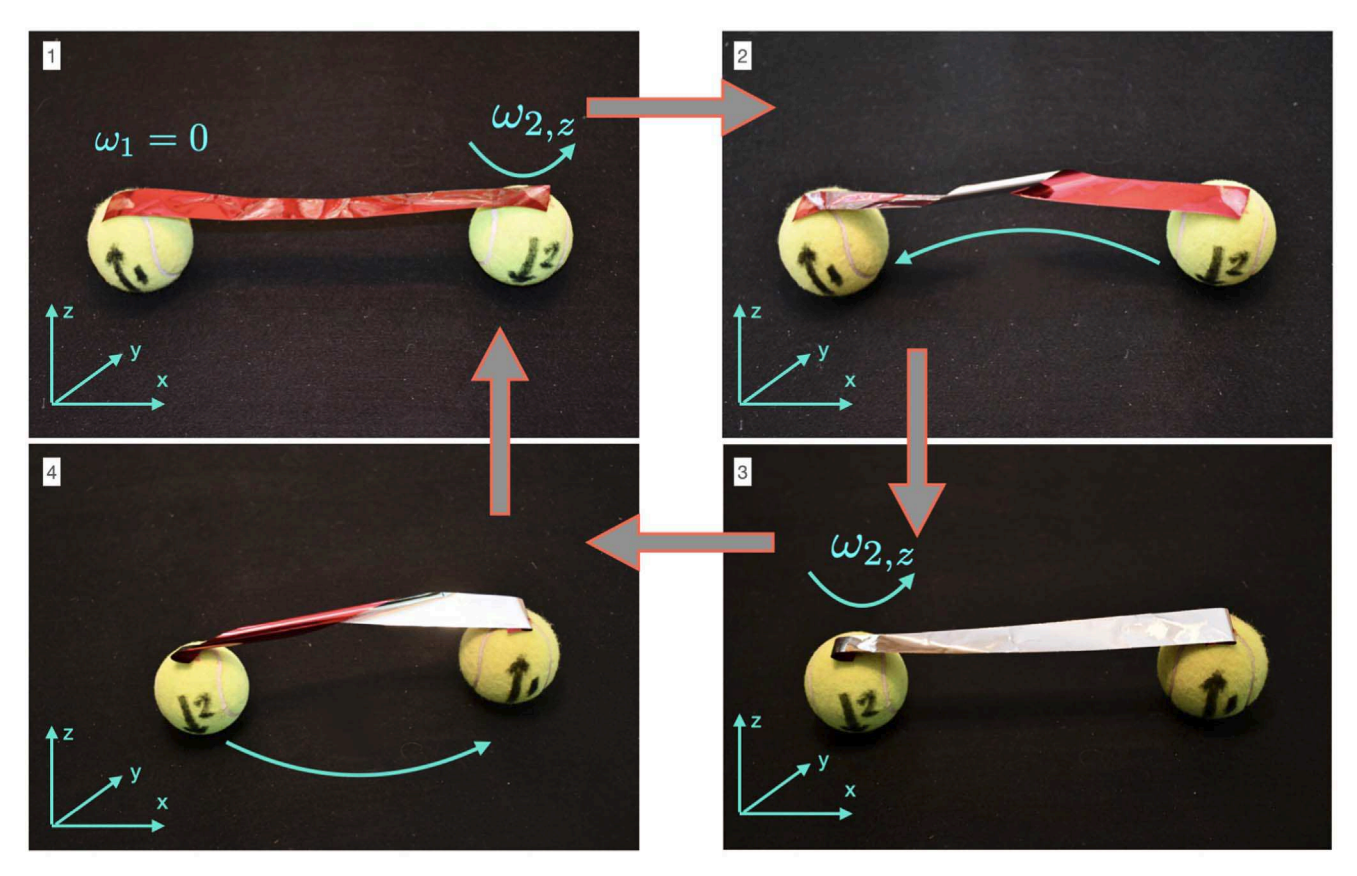


Figure 4. An example of the 2:1 spin-orbital resonance (Case II). The tennis balls represent two neutron stars. The black arrowindicates the direction of the magnetic moment. Two hemispheres (east and west) are clearly identified: this helps keep track of the spin phase. The ribbon is the magnetic field connecting the stars; magnetic moments are counter-aligned, so that there is a strong magnetic coupling between the stars. Star 1 is non-spinning. Star 2 first makes a full spin around the z-axis, which is orthogonal to the orbital plane, (panel 2), then half a rotation around star 1 (panel 3), then another full spin (panel 4), and another half orbital rotation brings it back to the initial configuration (panel 1). Such orbital untwisting of the common magnetosphere twisted by the spins occurs generically for many spins, orbital angular momentum, and magnetic moments directions.

Next, consider the case of spin of the second star along the y-axis. This case displays another property: topological bifurcation. For example, in Figure 7, the configuration unwinds, while in nearly equivalent case, Figure 8, it does not. Figure 9 illustrates this behavior.

#### 4. Topology of Field Winding

In addition to three globally untwisting structures (fully locked, same counter-aligned spins, and 2:1 beat-plus resonance) there are other configurations that untwist locally. We study conditions for such untwisting next. To this end, we first set up the geometric framework facilitating our search for non-winding configurations.

Our goal of studying the rate at which magnetic tubes are twisting is intimately related to topology. With this in mind, we discuss two convenient ways of thinking about magnetic tubes and then describe the topology of the relevant space, which can be viewed either as the rotation group  $\mathbb{F} = SO(3) = \mathbb{R}P^3$  (Section 4.2) or as the unit tangent bundle of a two-sphere  $\mathbb{F} = T^1S^2$  (Section 4.3).

#### 4.1. A Magnetic Tube

Let us start with a convenient mathematical description of a magnetic tube, it is a sufficiently small tubular neighborhood of some central magnetic line. It is formed by a smooth family of nearby magnetic lines parameterized by any transverse disk. (Mathematically, following the lines gives a diffeomorphism between any two transverse disks).

Consider a pair of disks<sup>3</sup>  $D_1$  and  $D_2$  (on the respective star surfaces) each oriented by a unit normal  $\vec{\mu}_1$  and  $\vec{\mu}_2$  directed along the magnetic field as in Figure 10. Their centers are connected by a length-parameterized path (representing a magnetic field line), the central line,

$$\beta \colon [0, \ell] \to \mathbb{R}^3$$

$$s \mapsto \beta(s), \tag{2}$$

with unit tangent  $\hat{B} = \frac{d\beta}{ds}$ . A nearby magnetic field line (dashed green) intersects a normal disk centered at  $\beta(s)$  at some point  $\beta(s) + n(s)$  and thus the shape of the nearby line is determined by a normal vector field n(s). Since we are only concerned with twisting, we keep track of the direction unit normal vector field  $\hat{n}(s) = n(s)/|n(s)|$ . We shall be concerned with how much one line twists around the other, or, rather, how this twisting is changing with time, as the two discs orbit each other while also spinning at the same time.

For now, let us focus on the static situation and describe the topology and geometry of a single magnetic tube, represented by a framed path  $(\beta, \hat{n})$  with given initial and final frames

 $<sup>\</sup>overline{}^3$  For global considerations,  $D_1$  is the magnetic north cap of star 1 and  $D_2$  is the magnetic south cap of star 2. For local considerations, these are small star surface disks centered on the beginning and end of some central magnetic line.

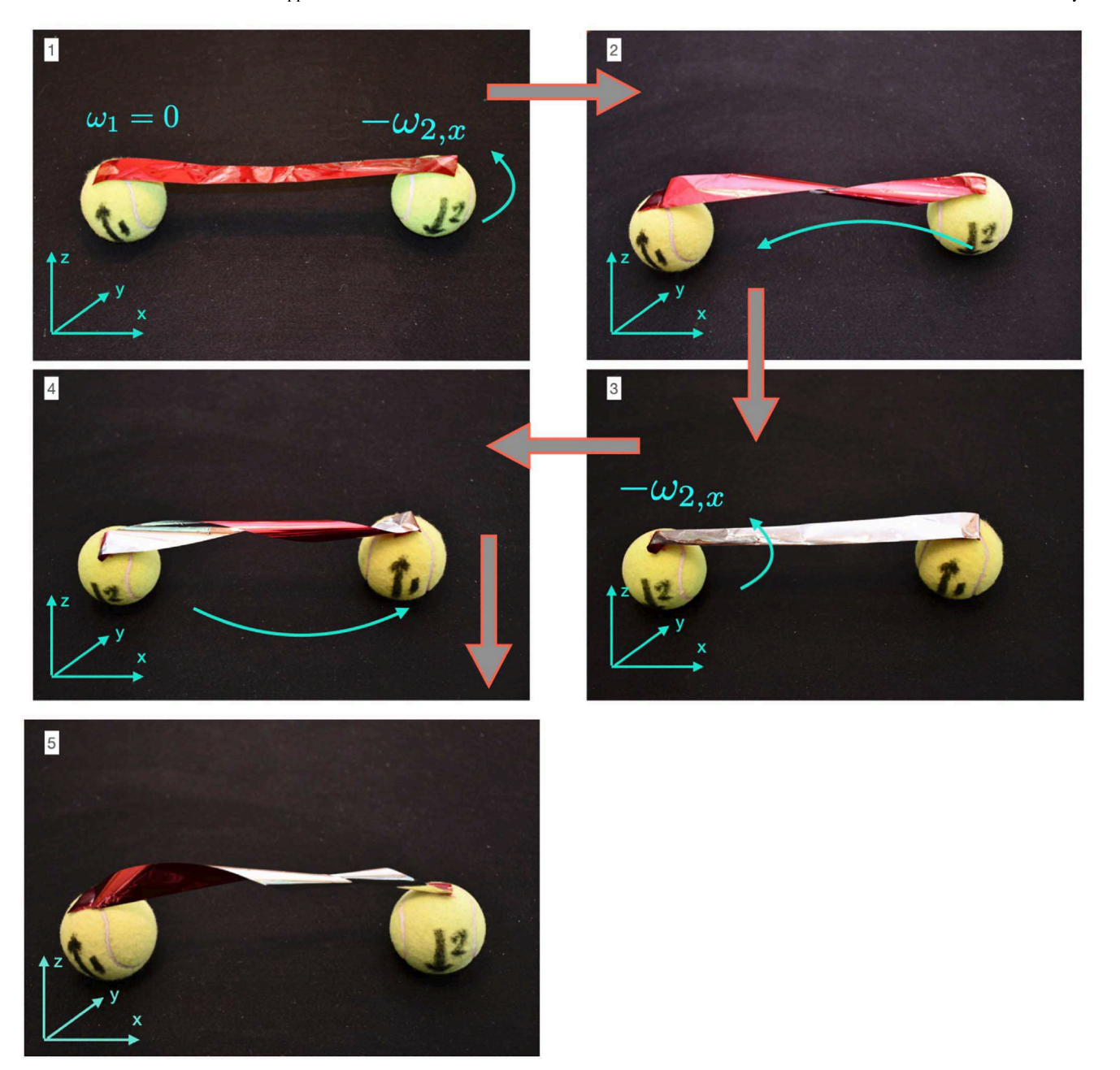


**Figure 5.** Second spin along the *x*-axis, with the second star undergoing two rotations during one orbital period. In this case the second star make one spin, then half an orbit, then another full spin, and then another half an orbit, the configuration *does not unwind*, see Figure 6.

specified by fixed  $\hat{B}(0) = \vec{\mu}_1$ ,  $\hat{B}(\ell) = \vec{\mu}_2$ , and fixed  $\hat{n}(0) = \hat{n}_1$  and  $\hat{n}(\ell) = \hat{n}_2$ .

## 4.2. Paths in SO(3)

The frame along a path  $\beta$  is specified by a single normal field  $\hat{n}(s)$ . Of course, the complete frame is formed by the triplet of vectors  $f = (\hat{B}, \hat{n}, \hat{B} \times \hat{n})$ . Written as a  $3 \times 3$  matrix, with each column representing a vector in this frame, we have an orthogonal matrix, thus a framed path gives a corresponding path in SO(3) with

$$f: [0, \ell] \to SO(3) \tag{3}$$

$$s \mapsto f(s) = (\hat{B}(s), \hat{n}(s), \hat{B}(s) \times \hat{n}(s)). \tag{4}$$

Thus, thinking of a small magnetic tube as a framed path, we arrive at a path f in SO(3). Clearly, the first column of f(s) is  $\hat{B}(s)$ , thus, the path  $\beta$  can be recovered from f via integration  $\beta(s) = \beta(0) + \int_0^s f(s)(1,0,0)^T ds$ .

Given two such framed paths  $(\beta, \hat{n})$  and  $(\beta', \hat{n}')$  with the same initial and final frames, one might ask whether it is possible to deform one of them into another, while holding the initial and final frames fixed. If it is indeed possible, then the corresponding paths f and f' in SO(3) are called homotopic. Thus it is worth understanding the space of paths in the group of orientation preserving rotations SO(3). Any rotation of  $\mathbb{R}^3$  can be specified by a single vector: its direction specified by the (oriented) axis of rotation and its length is the angle of the rotation around this axis. In particular, the length of this vector

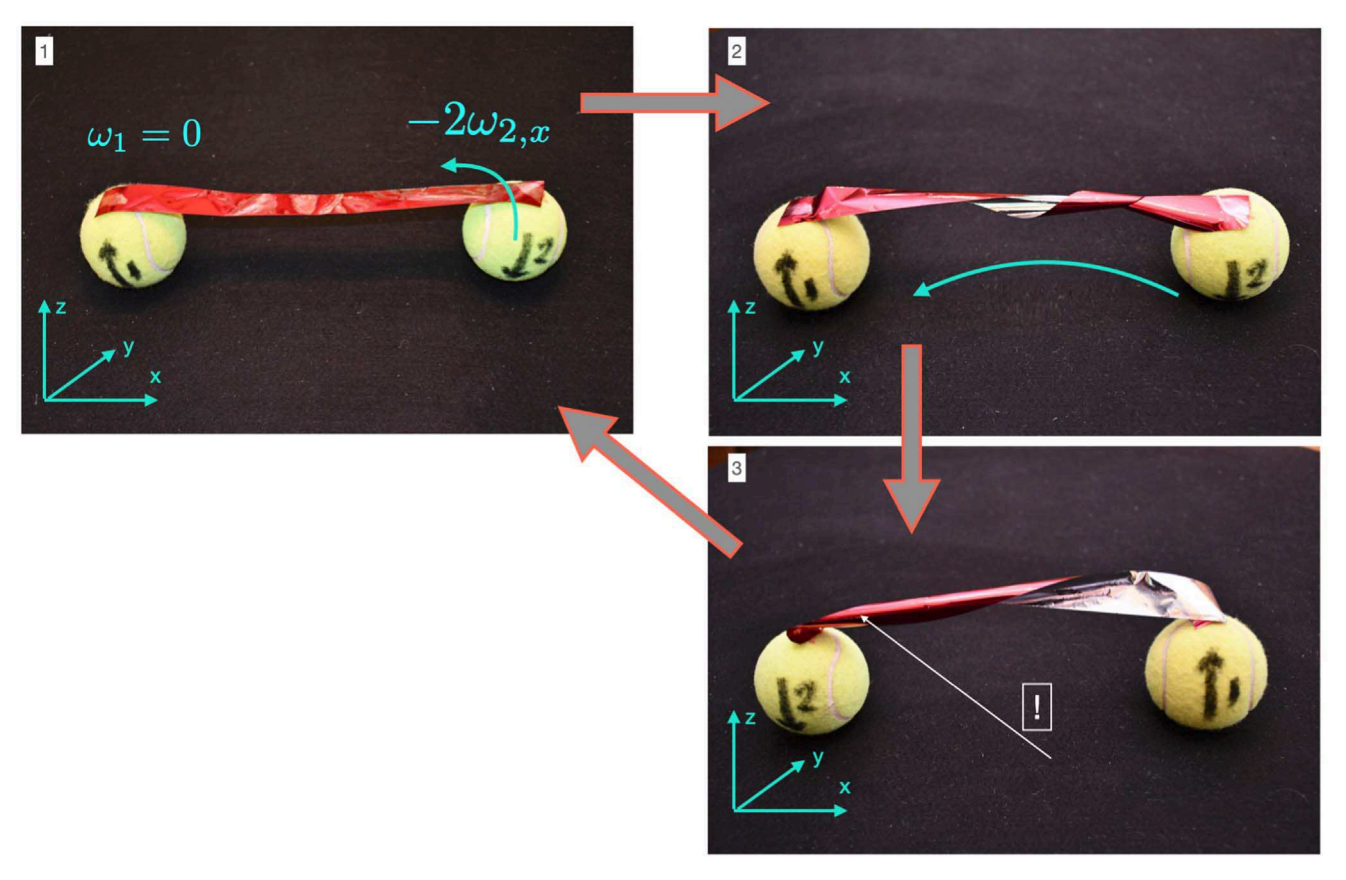


**Figure 6.** Second spin along the *x*-axis, with the second star undergoing two rotations during one orbital period. In this case, the second star makes two spin, then a full orbit, and the configuration *does unwind*, see Figure 8.

does not exceed  $\pi$ . At this stage, all rotations appear to be in one-to-one correspondence with a radius  $\pi$  ball in  $\mathbb{R}^3$ , except for one caveat. A rotation by angle  $\pi$  around  $\hat{m}$  produces the same result as a rotation by  $\pi$  around  $-\hat{m}$ , therefore the antipodal points on the surface of this ball correspond to the same rotation. One concludes that the group of rotations SO(3) is a three-ball with antipodal points of its surface identified.

One can view this three-ball as a northern hemisphere of some three-sphere  $S^3$ , making clear the identification of SO(3) with the three-dimensional projective space  $\mathbb{R}P^3 = S^3/\pm 1$ }, which is a three-sphere with its antipodal points identified (or, equivalently, the space of lines in  $\mathbb{R}^3$  passing through the origin):  $\mathbb{R}P^3 = SO(3)$ .

While a three-sphere is simply connected, i.e., any two paths between two given points can be deformed into each other, the projective space has exactly two classes of paths. The difference between the two paths is a closed path obtained by traversing the first path and then returning backward along the second path. This difference between the two paths in different classes is homotopic to (i.e., can be deformed to) the path in  $S^3$  connecting two of its antipodal points.

Note: the above is often illustrated with a belt, with its two ends held fixed at a distance, so that one can move the belt around these ends increasing or decreasing its twisting in the process. However, if one breaks the rules and twists one of the ends once, the resulting belt configuration differs from all prior ones, in that those cannot be reached by manipulating the belt, while its ends are held fixed.

The above correspondence is often interpreted in terms of spin. Namely, identifying SU(2) as a three-sphere (for example,

as a sphere of unit quaternions), and thinking of the three space  $\mathbb{R}^3$  as imaginary quaternions, the rotation R(M) of  $\mathbb{R}^3$  is a conjugation of the imaginary quaternions by a unit quaternion:  $SU(2) \ni M: x \mapsto M^{-1}xM$ . Then, clearly, M and -M have exactly the same effect on  $\mathbb{R}^3$  and the group of all orientation preserving rotations  $SO(3) = SU(2)/\pm 1$ . A framed path gives a path in SO(3) (for example starting at identity and arriving at some fixed frame  $M \in SO(3)$ ) and lifts unambiguously to a path in SU(2) (also beginning at identity). It will arrive at some element of  $\hat{M} \in SU(2)$ . As we deform the path in SO(3), its lift to SU(2) will still be beginning at identity and ending at  $\hat{M}$ . However, there is a whole other class of paths in SO(3) to M, they lift to paths in SU(2) from identity to  $-\hat{M}$ . Thus what governs the framed path (up to its deformations) is the spin group Spin(3) = SU(2), rather than SO(3). This is the reason a belt is sometimes used to illustrating fermion statistics.

#### 4.3. Paths in the Unit Tangent Bundle of a Two-sphere

Perhaps, a more economical view of a framed path is in terms of the tangent bundle  $TS^2$  of a two-sphere of directions  $S^2$ . This bundle consists of disjoint tangent planes to  $S^2$ . Namely, for any length-parameterized path  $\beta$  in  $\mathbb{R}^3$ , its normal tangents  $\hat{B} \colon [0, \ell] \to S^2$ ,  $s \mapsto \hat{B}(s) = \frac{d}{ds}\beta(s)$  form a path in the unit sphere  $S^2$  of directions, as in Figure 11, while  $\hat{n}(s)$ , orthogonal unit vector to  $\hat{B}(s)$ , is a tangent vector to  $S^2$  at  $\hat{B}(s)$ , as in Figure 12. Since it is normalized, it lies in the unit circle in the tangent plane  $T_{\hat{B}(s)}S^2$  to  $S^2$  at point  $\hat{B}(s)$ .

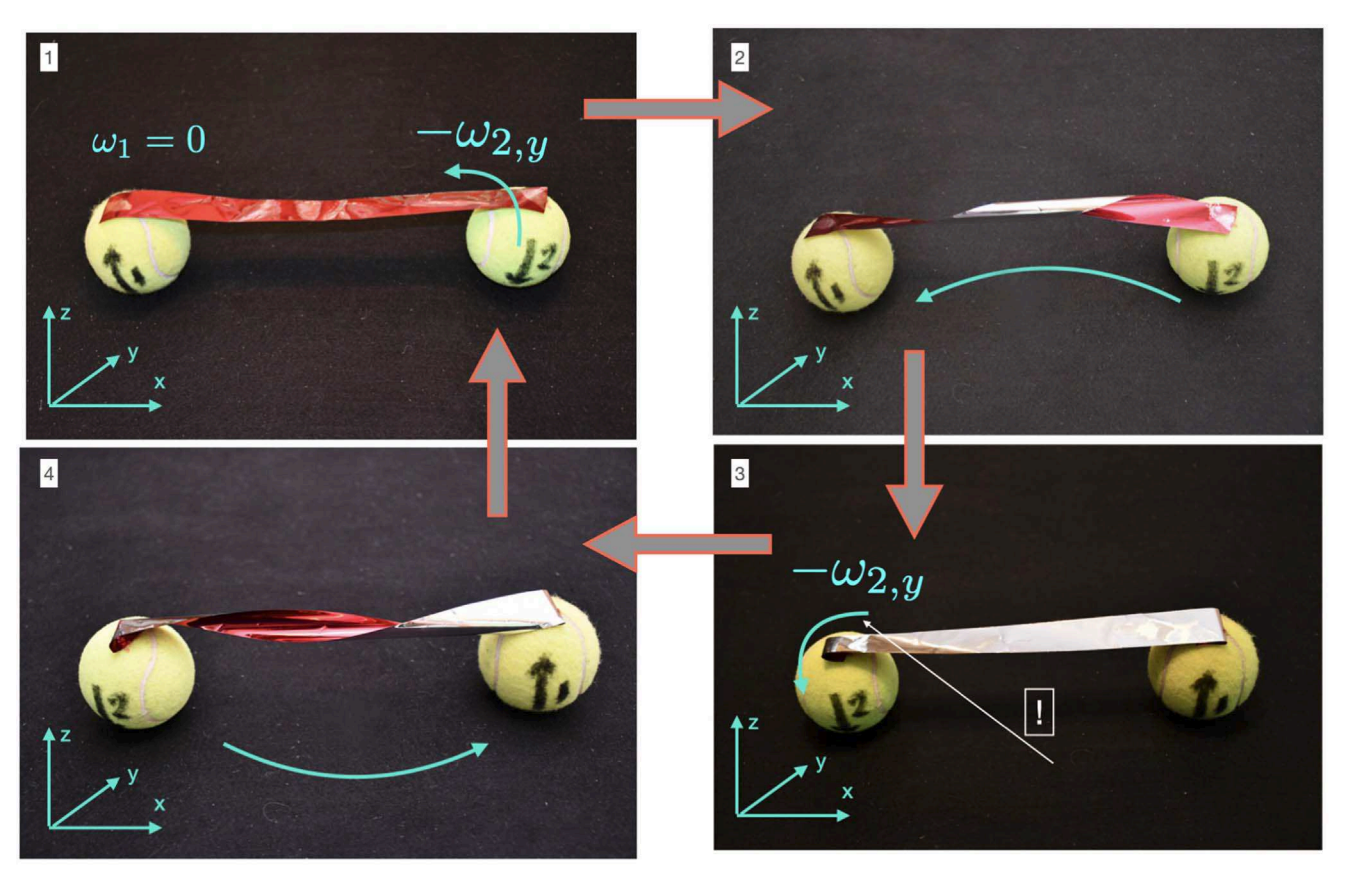


**Figure 7.** Second spin along the *y*-axis. First the second star makes a full spin, with the spin direction mostly along *y*-axis, but slightly misaligned in *positive x* direction. After half an orbital turn, the second star makes a full spin, with the spin direction mostly along *y*-axis, but slightly misaligned in *negative x* direction. The configuration unwinds.

Thus we arrive at a slightly different picture of the space  $\mathbb{F}$  of all unit circles in the tangent spaces of the unit two-sphere:  $\mathbb{F} = T^1S^2 \subset TS^2$ . An element of this space is specified by a pair (a, b) of orthogonal unit vectors, the first vector a specifies the point in  $S^2$  and the second vector b specifies a point in the tangent plane to  $S^2$  at a. Of course, given a point  $(a, b) \in \mathbb{F}$  the forgetful map  $(a, b) \mapsto a$  gives the corresponding element of the sphere; in other words, we have a natural projection  $\mathbb{F} \to S^2$ ,  $(a, b) \mapsto a$  (it projects a circle fiber of normals to its corresponding point on the sphere of directions).

A framed path  $(\beta, \hat{n})$  gives a path  $\beta$  in  $\mathbb{F}$  by

$$\hat{\beta} \colon [0, \ell] \to \mathbb{F}$$

$$s \mapsto (\hat{B}(s), \hat{n}(s)). \tag{5}$$

The path in the sphere traced by  $\hat{B}(s)$  simply traces out the directions of the path  $\beta$ , while the unit tangent field  $\hat{n}(s)$  along this path lifts it to  $\mathbb{F}$ . The path in the sphere begins at  $\vec{\mu}_1$  and ends in  $\vec{\mu}_2$ . It is constrained by  $\mathbf{R} = \int_0^\ell \hat{B}(s) ds$ . Thus, this path is bound to spend some time near  $\mathbf{R}/|\mathbf{R}| \in S^2$ , as illustrated in Figure 11. Needless to say, our description is equivalent to that of Section 4.2, as the space  $\mathbb{F}$  can be identified with SO(3) via  $(a, b) \mapsto (a, b, a \times b)$ .

Let us comment on the topology of the unit circle bundle  $T^1S^2$  of the two-sphere  $S^2$ . In particular, we would like to make it transparent that it is a degree 2 Hopf bundle. This degree 2 is at the heart of the effect discussed in this paper; it is responsible

for the persistence of the 2:1 resonance. Perhaps the most common way to demonstrate that the degree is 2 is to consider the polar projection  $F: S \setminus \{N\} \to \mathbb{R}^2$  from the north pole N to the plane tangent at the south pole S. Taking a constant vector field on the plane and pulling it back to  $S \setminus \{N\}$  one obtains a vector field that winds twice as one circumnavigates the north pole traversing a small meridian near it.

For our purposes, however, we use a different picture, illustrated in Figure 13. We trivialize the bundle over the northern hemisphere  $U_{\rm N}$ , the southern hemisphere  $U_{\rm S}$ , and over the tropical region  $U_{\rm T}=S^2\setminus\{N,S\}$  containing the equator, as follows. Let us mark a point E on the equator and call it the east pole. We also call its antipodal point the west pole. A unit tangent vector field u directed toward E is then well defined everywhere on the sphere except at E and at W. We use it to define coordinates in the tangent circle fiber over  $U_{\rm N}$  and  $U_{\rm S}$ . For any point  $p\in U_{\rm N}$  and for any tangent unit vector  $w_p$  at p, let  $\phi_{\rm N}(w_p)$  be the angle between  $u_p$  and  $w_p$ . Now, any real number determines a unique unit tangent vector at p, whose angle with  $u_p$  is that number. In other words, we defined a coordinate along the circle fiber. Similarly, if  $p\in U_{\rm S}$ , we define  $\phi_{\rm S}(w_p)$  to be the angle between  $u_p$  and  $w_p$ .

Next, consider the northward unit tangent field v. It is well defined everywhere in the tropical region  $U_T$ . For any  $p \in U_T$  let  $\phi_T(w_p)$  be the angle between  $v_p$  and  $w_p$ .

Consider some parallel in the Northern hemisphere and a point p on it. Clearly,  $\phi_T = \phi_N + \phi_T(v_p)$ , i.e., the difference between the two angles  $\phi_T(w_p)$  and  $\phi_N(w_p)$  is the angle between

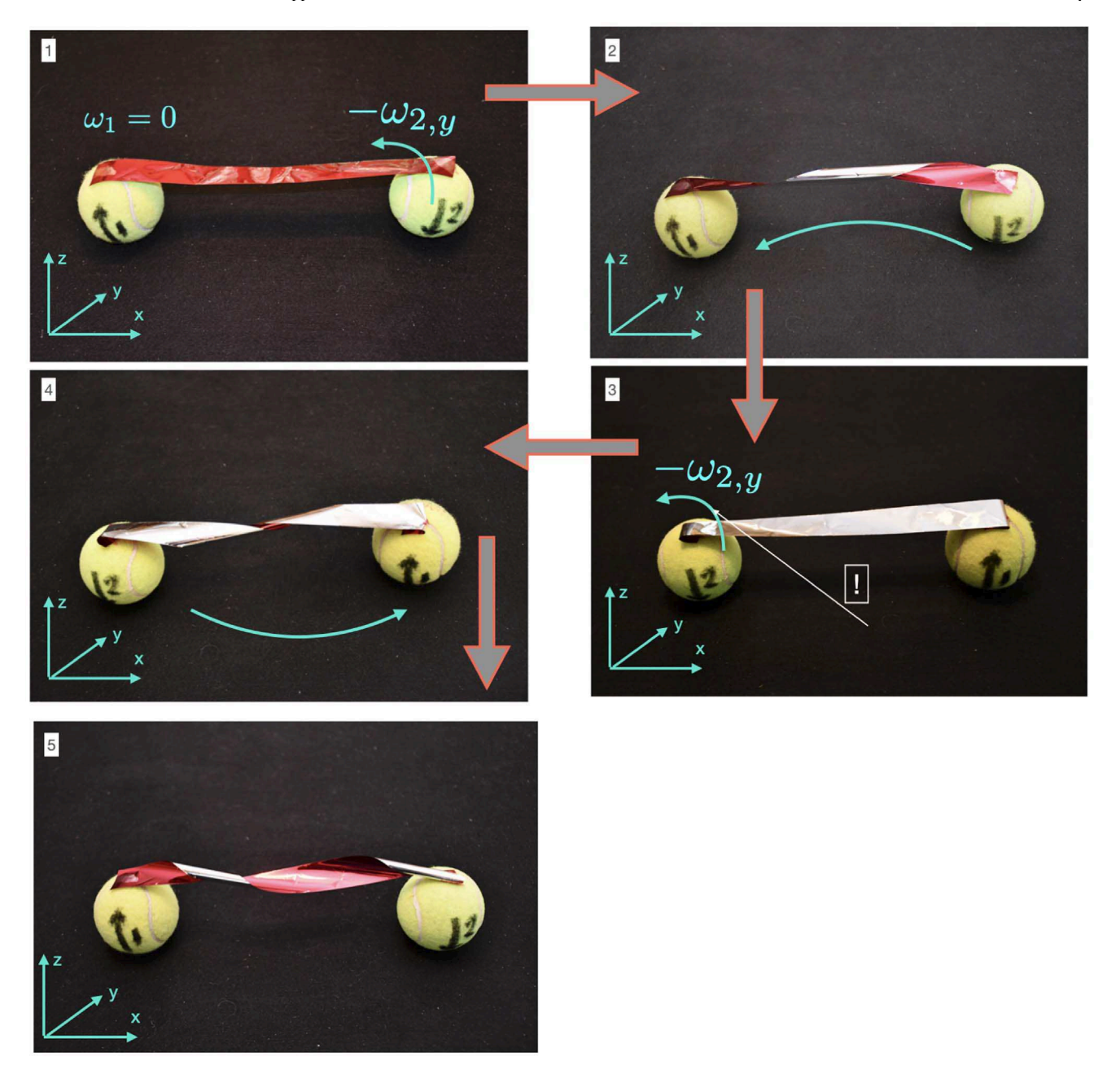


**Figure 8.** Second spin along the y-axis. First the second star makes a full spin, with the spin direction mostly along y-axis, but slightly misaligned in the positive x direction. After half an orbital turn, the second star makes a full spin, with the spin direction mostly along y-axis, but slightly misaligned also in positive x direction. The configuration does not unwind.

 $v_p$  and  $u_p$ . Whenever the point p circumnavigates the parallel eastward, this angle between  $v_p$  and  $u_p$  changes by  $2\pi$ , i.e.,  $\Delta(\phi_{\rm T}(w_p)-\phi_{\rm N}(w_p))=2\pi$ . Similarly, circumnavigating any parallel in the southern hemisphere eastward, the change in the difference between  $\phi_{\rm T}$  and  $\phi_{\rm S}$  is  $-2\pi$ , i.e.,  $\Delta(\phi_{\rm T}(w_p)-\phi_{\rm S}(w_p))=-2\pi$ .

For example, if we have a path in  $\mathbb{F}$  passing over the equator, then, if we move it all the way around the equator holding the limiting value of, say,  $\phi_N$  at the equator fixed, then the value of  $\phi_E$  will change by  $2\pi$ , while the value of  $\phi_S$  will change by  $4\pi$ . It is this factor of 2 in  $2\times 2\pi$ , that is the *degree* or the *Hopf number* of this bundle. (It is exactly because this degree is not zero that the sphere "cannot be combed," i.e., it has no nowhere vanishing continuous tangent fields. It is also the reason there is no global coordinate along the fiber of  $\mathbb{F}$ .)

#### 4.4. Relative Twisting

For some paths, one might be able to introduce the notion of twisting, for example, using the (unit) tangent  $\hat{B}$  and curvature  $d\hat{B}/ds$  of the path to form a frame along it. Such a Frenet frame could be used to define the twisting of a magnetic tube centered around that path. However, as we consider the evolution of the path, as it changes its shape, we might (and even are likely to) loose this frame. For example, the curvature might vanish at some point. This would prevent continuous tracking of this path twisting angle. In other words, there are two issues preventing us from discussing twisting of an arbitrary tube:

1. there cannot be a coordinate on the fiber circle that is valid over the whole sphere of directions and

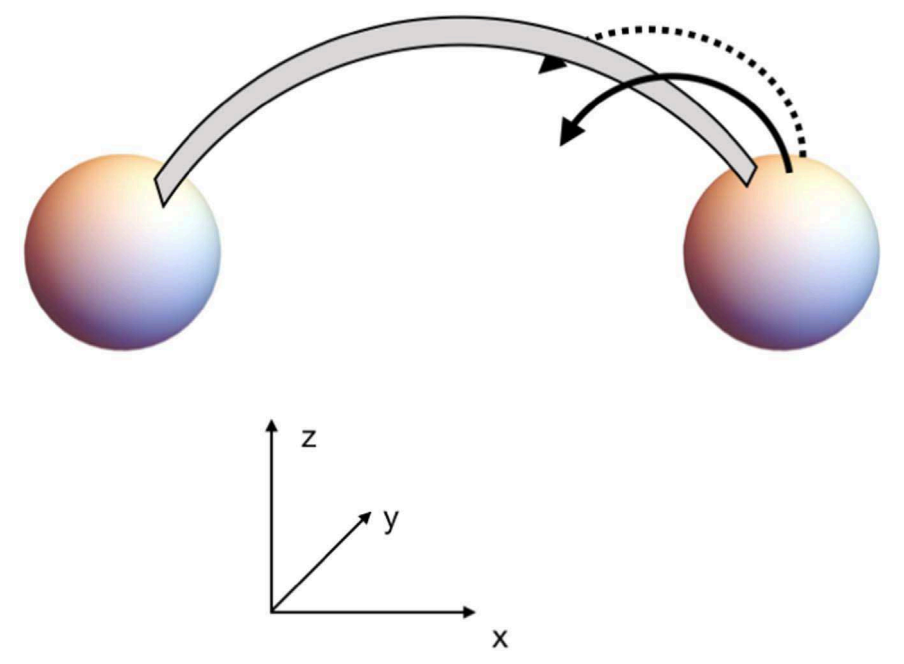


**Figure 9.** Topological bifurcation. The star on the right spins approximately along the y-axis (which is into the board). Small variations of the spin direction would result in different topological behaviors: one not resulting in winding, another resulting in winding.

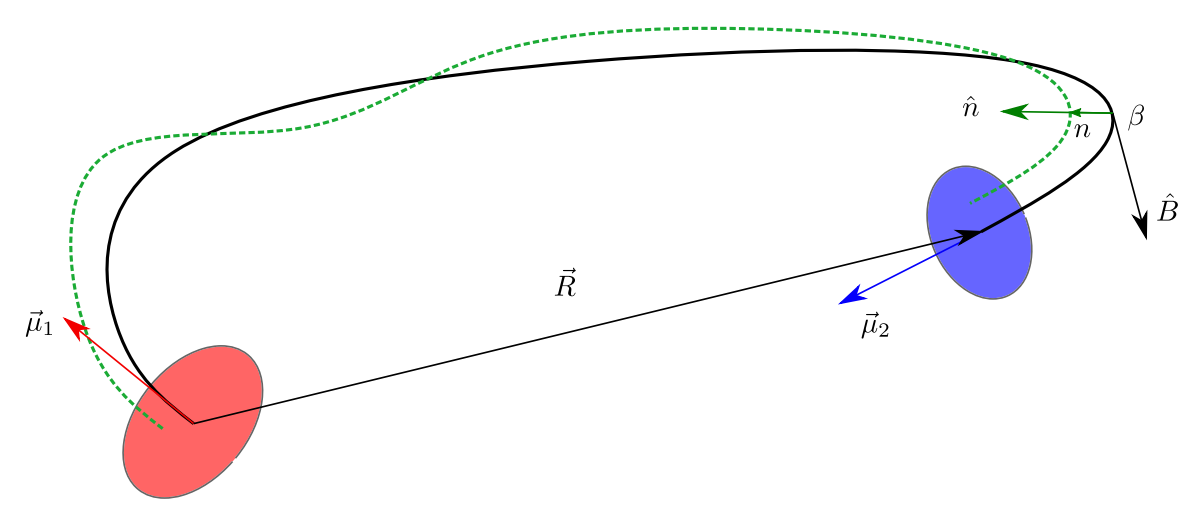


**Figure 10.** The central magnetic line in black connects the two disks on the stars' respective surfaces. A nearby magnetic line is the dashed green line with separation vector n(s) and separation direction  $\hat{n}(s)$ .

2. there is no guarantee that the path of directions  $\hat{B}$  is differentiable, even though the original path in  $\mathbb{R}^3$  was.

However, if we have one path  $\hat{\gamma}_1$  and another path  $\hat{\gamma}_2$  in  $T^1S^2$ , and both happen to project to the same path  $\gamma$  in  $S^2$ , then there is a good notion of how much  $\hat{\gamma}_2$  winds around  $\hat{\gamma}_1$ . To do this, as we traverse  $\gamma$ , we continuously track the change in the angle between  $\hat{\gamma}_1(s)$  and  $\hat{\gamma}_2(s)$ . Importantly, this does not involve any charts, fiber coordinates, or auxiliary vector fields. Thus, for such a pair of paths, the relative twisting angle is well defined.

In general, we shall consider a family of framed paths  $\hat{\gamma}(s, t)$ , where s is the length parameter along a path at time t. In particular,  $\hat{\gamma}(s, 0) = \hat{\gamma}_1(s)$  is the initial path and  $\hat{\gamma}(s, 2\pi) = \hat{\gamma}_2(s)$  is the final path. Also, the projection of  $\hat{\gamma}(s, t) \in \mathbb{F}$  is the direction  $\gamma(s, t)$ .

Let us begin with a very simple example, consider a path  $\gamma(s, t)$  that is the meridian from N to S with longitude t. Clearly, as t changes from 0 to  $2\pi$ , this meridian sweeps the sphere and

returns to its original shape, i.e.,  $\gamma(s,0)=\gamma(s,2\pi)$ . Consider a tangent vector field to each meridian that, away from a small neighborhood of the equator is given by the east pole directed field v. (Clearly, the field v does not give a good normal field along the whole family  $\gamma(s,t)$ , since it is not defined at E and W. Thus, for each t, we interpolate the resulting tangent field along the path  $\gamma(s,t)$  in the vicinity of the equator.) Let  $\hat{\gamma}(s,0)$  be the path lifting the meridian  $\gamma(s,0)$  using that field (outside the neighborhood of the equator) and continuous along the whole meridian. As we vary t and the meridian  $\gamma(s,t)$  rotates sweeping the sphere, we keep  $\hat{\gamma}(s,t)$  given by v away from the equator and change continuously with s and t. We would like to learn about the resulting path  $\hat{\gamma}(s,2\pi)$  relation to the original path  $\hat{\gamma}(s,0)$ .

In terms of the local coordinates, these paths have  $\phi_N=0$  and  $\phi_S=0$  away from the neighborhood of the equator. There is a discontinuity between  $\phi_N$  and  $\phi_T$ , for example, and this discontinuity changes by  $2\pi$  as the meridian sweeps the sphere.

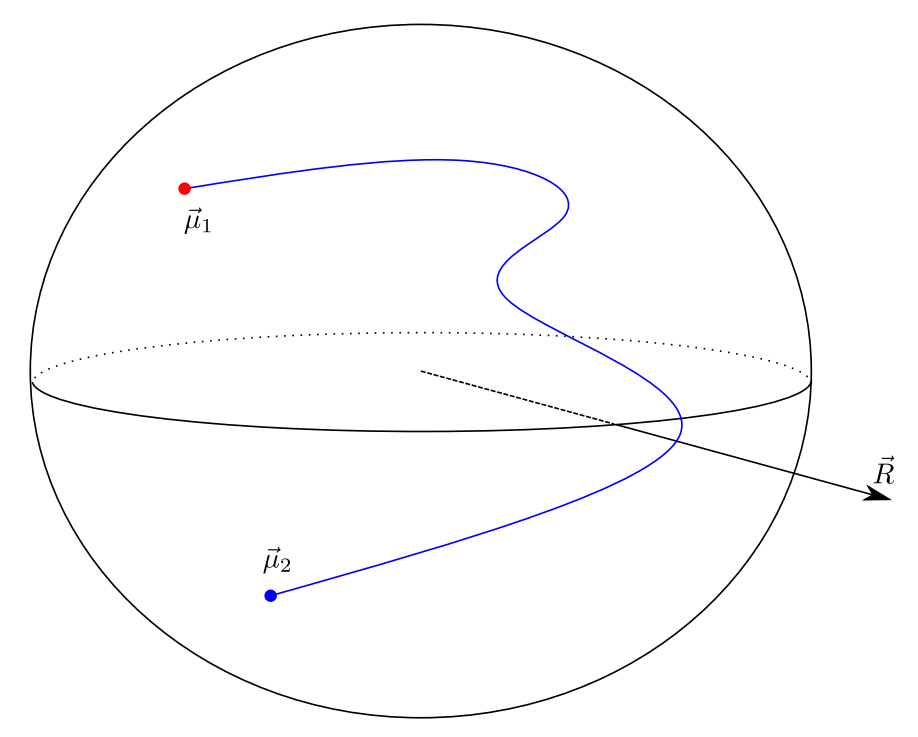


**Figure 11.** A single magnetic line (with displacement R) is represented by a blue path in the sphere of directions (satisfying  $\int_0^\ell \hat{B}(s) ds = R$ ).

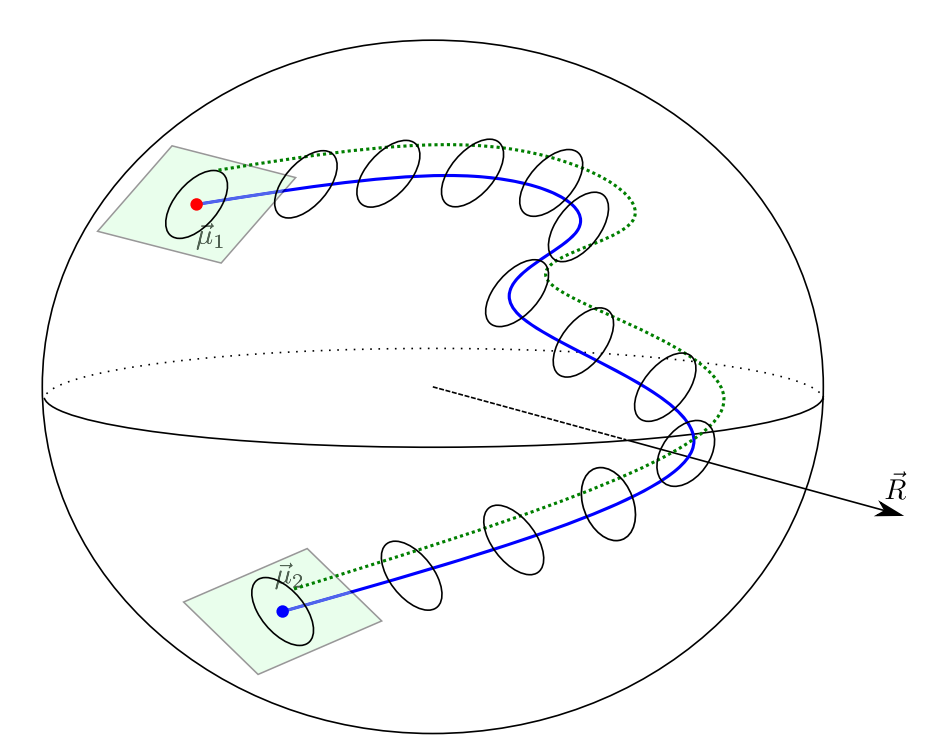


Figure 12. A magnetic tube is represented by the green dashed path in  $\mathbb{F}$ , which is equivalent to a unit tangent vector field along the blue solid line.

Since we keep the north and south coordinates zero by construction, and the gap between  $\phi_{\rm N}$  and  $\phi_{\rm T}$  changes by  $2\pi$ , the interpolating path near the equator has to adjust, changing its initial value of  $\phi_{\rm T}$  just north of the equator. Similarly, since the gap between  $\phi_{\rm T}$  and  $\phi_{\rm S}$  changes by  $2\pi$ , the value of  $\phi_{\rm T}$  just south of the equator changes. As a result, the interpolating part of the path shown in dashed blue in

Figure 14 wraps twice around the fiber relative to the original path shown in solid red.

In fact, nothing in this argument depends on our special choice of path lifting, so long as we hold the initial and final frames fixed. (The solid red and dashed blue graphs in Figure 14 will be arbitrary, but the relation between their discontinuities will remain the same, adding up to  $4\pi$ .) As the

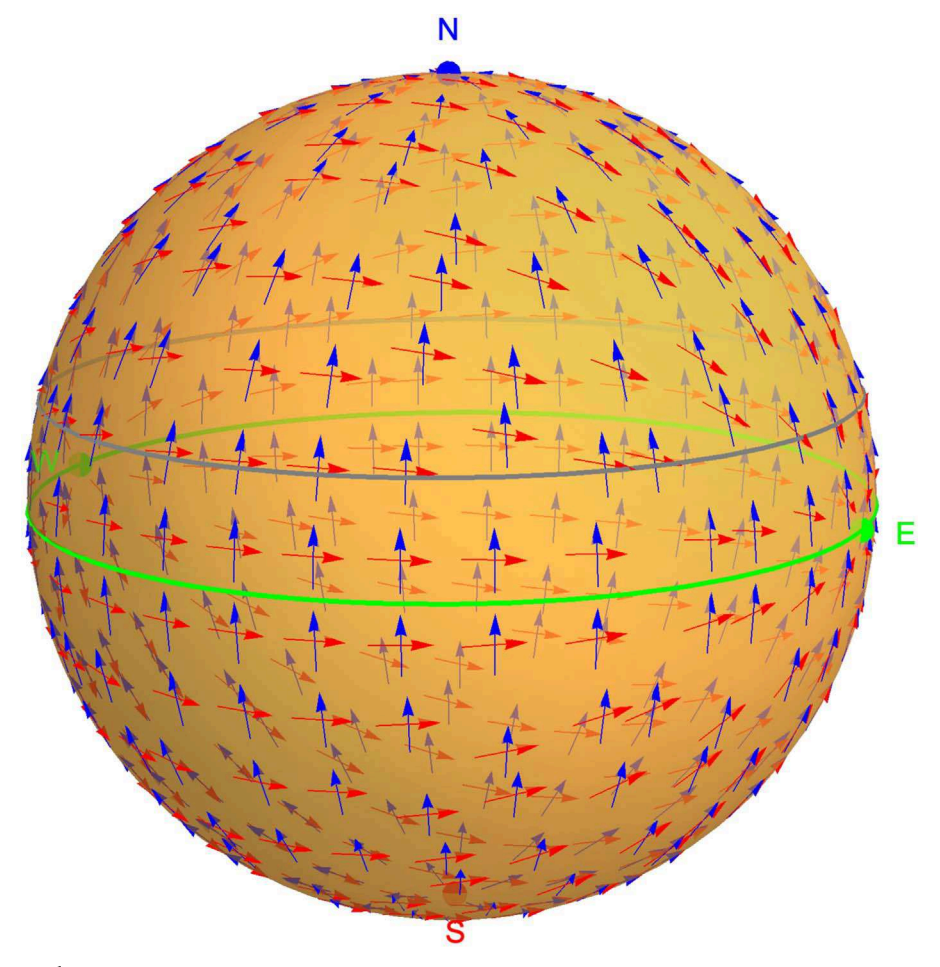


Figure 13. The vector field v is in blue is due north and the field u in red is directed toward the East pole. As one circles eastward along the gray parallel, v rotates once counterclockwise relative to u.

path  $\gamma$  sweeps the sphere once (moving eastward), the path  $\hat{\gamma}(s, 2\pi)$  will twist by  $4\pi$  relative to  $\hat{\gamma}(s, 0)$ .

#### 4.5. Case Redux

With our newly gained perspective, let us revisit the cases discussed in Section 3 and account for the observed twisting.

Case I had  $\vec{\omega}_1 = \vec{\omega}_2 = \vec{\Omega} \sim \hat{z}$ . In terms of the sphere of directions this can be visualized (Figure 15 left panel), as points  $\vec{\mu}_1$  and  $\vec{\mu}_2$  presented as, respectively, red and blue dots circling in the same (eastward) direction around, respectively, north and south poles. The path of directions is the blue path on the sphere connecting these two points and passing in the vicinity of the black dot  $\hat{R}$ . The latter rotates around the equator. The twisting is captured by the sum of the angles  $\chi_1$  and  $\chi_2$ . For Case I, all three points (red, blue, and black) rotate with the angular velocity, and the resulting angles  $\chi_1$  and  $\chi_2$  can remain constant. Therefore, we observe no winding.

Case II, as illustrated in Figure 2, is very similar to the picture above. As illustrated in the right panel of Figure 15, the red and blue dots moving in the opposite directions (with equal angular velocity), while the black bot is staying put. In this case, one of the  $\chi$  angles increases, while another decreases, with their sum remaining constant (on average). Therefore, there cannot be twisting in this case.

Case II, as illustrated in Figure 3, is the picture we just described, but rotated, so that now the blue dot is staying put,

the black dot rotates, and the red dot rotates twice as fast. This modification has no bearing on the resulting evolution of the angles  $\chi_1$  and  $\chi_2$ , again resulting in no winding.

In the remaining cases, Figures 5–8,  $\vec{\omega}_1 = 0$  and the red dot stays put at the north pole. Clearly, for actual continuous spin and orbital motions, there is no difference between  $\vec{\omega}_2$  directed along the x- or along the y-axis, due to the rotational symmetry. In the table-top demonstrations, however, the motions are consecutive and the result depends on their order. For example, Figure 5 movements in terms of the direction the two-sphere example on the left of Figure 16, amount to the blue point circling along the vertical meridian (winding = -1), then the original black dot  $\hat{R}(1)$  moving along the equator to  $\hat{R}(3)$  (winding = -1+1), the blue point circles the meridian again (with  $\hat{R}$ ) on the other side (winding = -1+1+1), and the blue point completing its journey around the equator (winding = -1+1+1+1).

The movements of Figure 6, on the other hand, consist of the blue point circling the meridian twice (winding = -2) followed by the black dot circling the equator (winding = -2+2).

The case of  $\vec{\omega}_2$  aligned with the y-axis presents a bifurcation, since in this case, the blue point passes through the black point. This is the moment of bifurcation. Movements of Figure 8 (with  $\vec{\omega}_2 = \omega_2 \hat{y} + \epsilon \hat{x}$ ) from the two-sphere of directions point of view are not so different from those of Figure 5 discussed above. The only difference is that the vertical meridian is

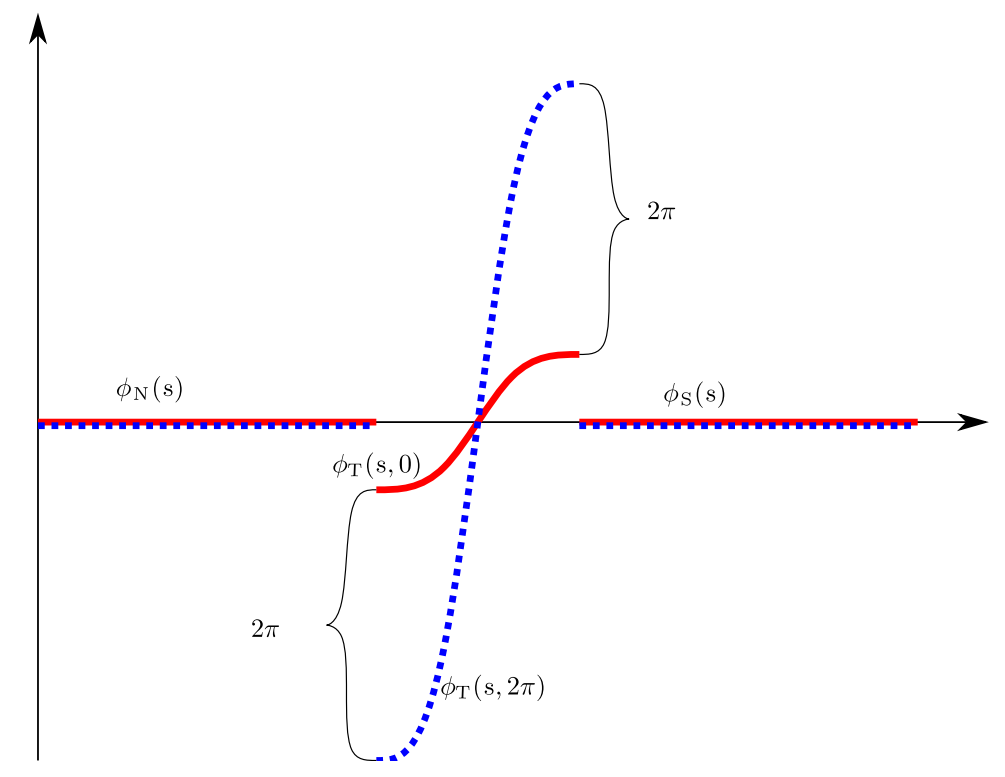


Figure 14. Local fiber coordinate of the initial path in solid red and of the final path in dashed blue. North and South patch coordinates  $\phi_N(s, t)$  and  $\phi_S(s, t)$  are held fixed and equal to zero.

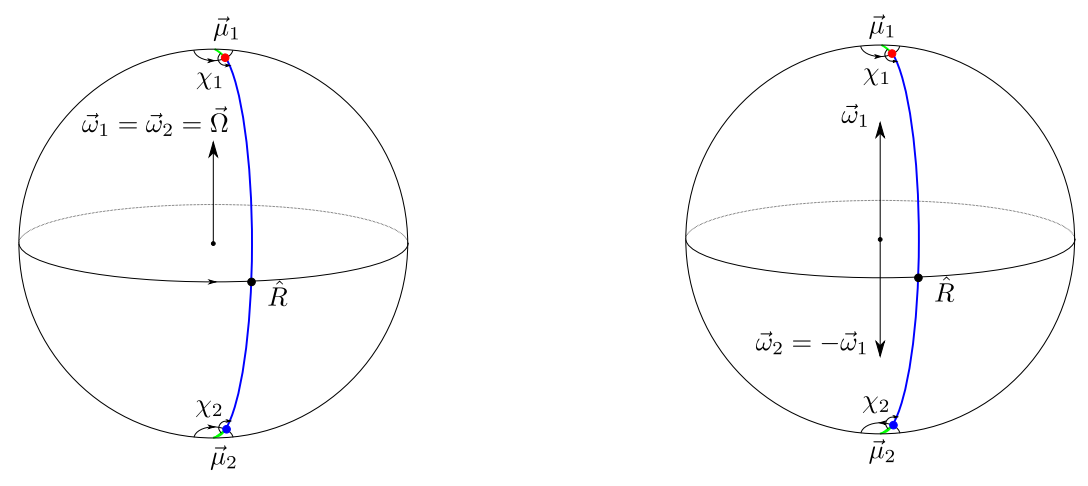


Figure 15. Cases I and II in terms of the unit two-sphere of directions. Left corresponds to Case I and right corresponds to Case II illustrated in Figure 2 (rotation of this right figure illustrates Figure 3). All have no winding of magnetic tubes.

rotated to the green meridian in Figure 16. The winding calculation remains the same.

Movements of Figure 7 result in the blue point circling the green meridian (winding =-1), the black point moving along the equator from  $\hat{R}(1)$  to  $\hat{R}(2)$  (winding =-1+1), then the blue point circling the orange meridian (winding =-1+1-1), and the black point completing its trip around the equator (winding =-1+1-1+1).

### 4.6. Twisting Rate of the Magnetic Tube

If we keep the central line fixed and rotate the first disk in Figure 10 around its axis once, the new green path will wind by  $2\pi$  relative to the original green path. Similarly, rotating the second disk once winds this path by  $-2\pi$ . All the action in

these cases is taking place in the cylinder in  $\mathbb{F} = T^1 S^2$  that is the preimage of the blue direction path.

Another important effect is due to the orbital motion, namely the point  $\hat{R} = R/|R|$  is rotating around the equator with frequency  $\Omega$ . Let us first focus on the path of directions in the sphere  $S^2$  while holding its origin  $\vec{\mu}_1$  and its end  $\vec{\mu}_2$  fixed. Moreover, we presume that  $\vec{\mu}_1$  is in the northern hemisphere and  $\vec{\mu}_2$  is in the southern hemisphere. As discussed in Section 4.3, the path of directions passes in the vicinity of  $\hat{R}$ , as illustrated in Figure 11. As a result, during one orbital rotation, the path of directions sweeps the whole surface of the sphere, and the magnetic tube twisting angle will increase by  $4\pi$  with each such sweep.

Since the main phenomenon we are describing is topological in nature, we can simplify our path of directions by deforming

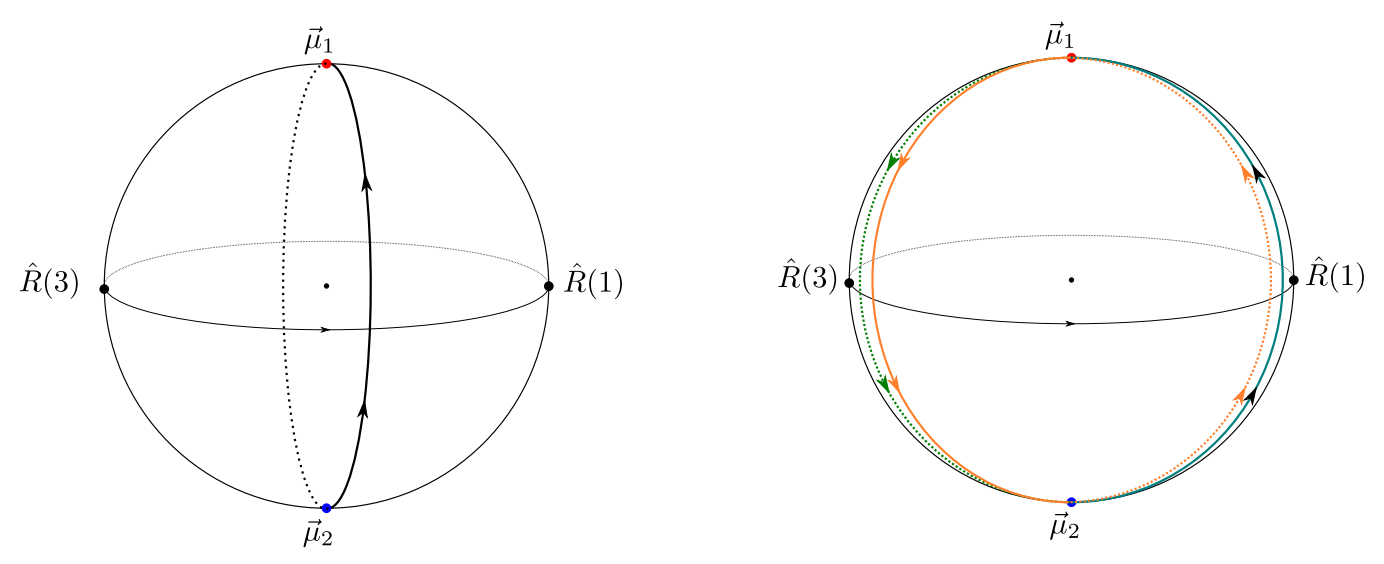


Figure 16. The left figure illustrates the sequence of moves of Figures 5 and 6, with consecutive moves of  $\vec{\mu}_2$  around the vertical meridian and movements of  $\hat{R}$  around the equator. The right figure illustrates the moves of Figures 8 and 7, with Figure 8 involving  $\vec{\mu}_2$  circling the green meridian both times and Figure 7 involving  $\vec{\mu}_2$  circling the green and then the orange meridian.

it to be the major arc from  $\vec{\mu}_1$  to  $\hat{R}$  followed by the major arc from  $\hat{R}$  to  $\vec{\mu}_2$ . (For example we can deform the blue path of directions to the arc path just described, without passing through the antipodal point  $-\hat{R}$ .) During this deformation, the covering path (dashed blue) will deform as well. In fact, we deform it so that at  $\hat{R}$  the tangent vector is pointing due north. Any such choice does not change the twisting, since rotating the tangent vector at  $\hat{R}$  by some angle  $\phi$  twists one part of the tube by  $-\phi$ , while twisting the other by  $\phi$ , thus not changing the total path twisting at all.

This deformation makes it very easy to track the tube winding and its time evolution. In fact, now that the frame at  $\hat{R}$  is fixed, we have a separate notion of twisting of the first part of the path and of its second part. In particular, if  $\vec{\mu}_1 \in U_N$  and  $\vec{\mu}_2 \in U_S$ , then as  $\hat{R}$  circumnavigates the equator, the northern part winds by  $2\pi$ , and so does the southern part. Let us put this more geometrically. When the point  $\hat{R}$  rotates around  $\vec{\mu}_1$  counterclockwise, the  $\vec{\mu}_1 - \hat{R}$  path segment is twisted by  $2\pi$ . Similarly, whenever,  $\hat{R}$  moves around  $\vec{\mu}_2$  clockwise the segment  $\hat{R} - \vec{\mu}_2$  is twisted by  $2\pi$ . (Note, the difference is due to the opposite orientation:  $\vec{\mu} - \hat{R}$  versus  $\hat{R} - \vec{\mu}$ ).

Now, as the path of directions returns to itself after one orbital rotation, what happens to the magnetic flux tube? It is twisted by  $4\pi$  if  $\vec{\mu}_1$  is north of equator and  $\vec{\mu}_2$  is south of it. It is twisted by  $-4\pi$  if  $\vec{\mu}_1$  is south of equator and  $\vec{\mu}_2$  is north of it. And it is not twisted at all if  $\vec{\mu}_1$  and  $\vec{\mu}_2$  are on the same side of the equator. This effect of the orbital motion is due to the fact that the bundle  $\mathbb F$  of circles over the sphere has Hopf number 2.

Of course in general the disks will spin and orbit each other at the same time. Consider the first disk rotating with angular velocity  $\vec{\omega}_1$  and the second with angular velocity  $\vec{\omega}_2$ . Then, the points  $\vec{\mu}_1$  and  $\vec{\mu}_2$  will be in circular motions around  $\hat{\omega}_1 = \frac{\vec{\omega}_1}{\omega_1}$  and  $\hat{\omega}_2 = \frac{\vec{\omega}_2}{\omega_2}$ , respectively. Let  $\alpha_1$  be the angle between  $\vec{\Omega}$  and  $\vec{\omega}_1$  and let  $\beta_1$  be the angle between  $\vec{\omega}_1$  and  $\vec{\mu}_1$ , as in Figure 17. Similarly, we define  $\alpha_2$  and  $\beta_2$  using  $\vec{\omega}_2$  and  $\vec{\mu}_2$ . Now, as the first disk undergoes one such rotation around  $\omega_1$ , it rotates around its axis once, therefore, as  $\vec{\mu}_1$  undergoes one rotation around  $\frac{\omega_1}{|\omega_1|}$ , the

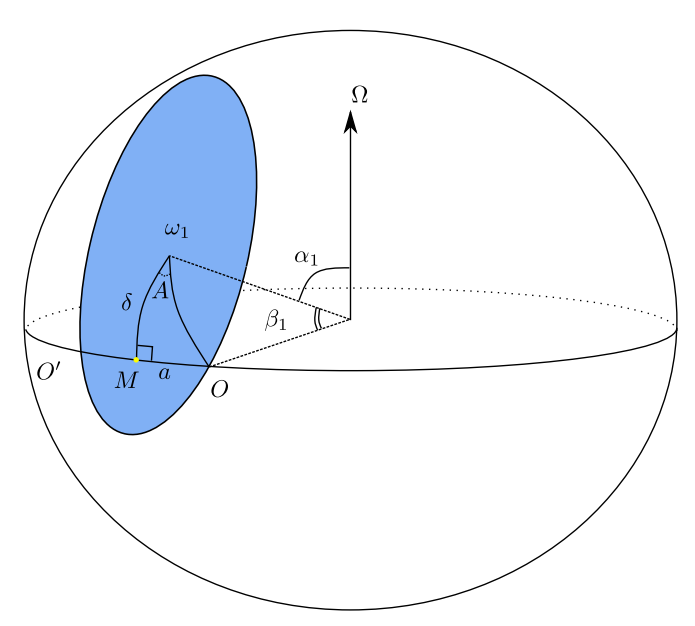


Figure 17. The blue spherical disk is centered at  $\hat{\omega}_1$  and bounded by the trajectory of  $\hat{\mu}_1$ . Its opening angle is  $\beta_1$ . The spherical triangle  $\triangle \omega_1 MO$  supports one-half of the equatorial arch between the two points O and O' where the orbit of  $\hat{\mu}_1$  crosses the equator. The angle  $\angle O\omega_1 M$  is denoted by A, while the length of its opposing side MO is a.

circle fiber of  $\mathbb{F}$  above it rotates once (relative to the fiber at  $\hat{\omega}_1$ ). The resulting twisting, however, depends on whether  $\mathbf{R}$  lies inside or outside the smaller disk bounded by the circle traversed by  $\omega_1$  (or, respectively,  $\omega_2$ ; see Figures 18 and 19).

#### 4.7. Effective Rate of Twisting

If the motion of  $\vec{\mu}_1$  is happening entirely in one hemisphere (either northern or southern) and the same holds for  $\vec{\mu}_2$ , then the twisting rate of the  $\hat{\mu}_1 - \hat{R}$  part is  $-\omega_1 \operatorname{sign} \vec{\omega}_1 \cdot \vec{\mu}_1 + \Omega \operatorname{sign} \vec{\Omega} \cdot \vec{\mu}_1$ , while the twisting rate of the  $\hat{R} - \hat{\mu}_2$  part is  $-\omega_2 \operatorname{sign} \vec{\omega}_2 \cdot \vec{\mu}_2 + \Omega \operatorname{sign} \vec{\Omega} \cdot \vec{\mu}_2$ . Assembling the two together, we have the rate of twisting of the whole path:

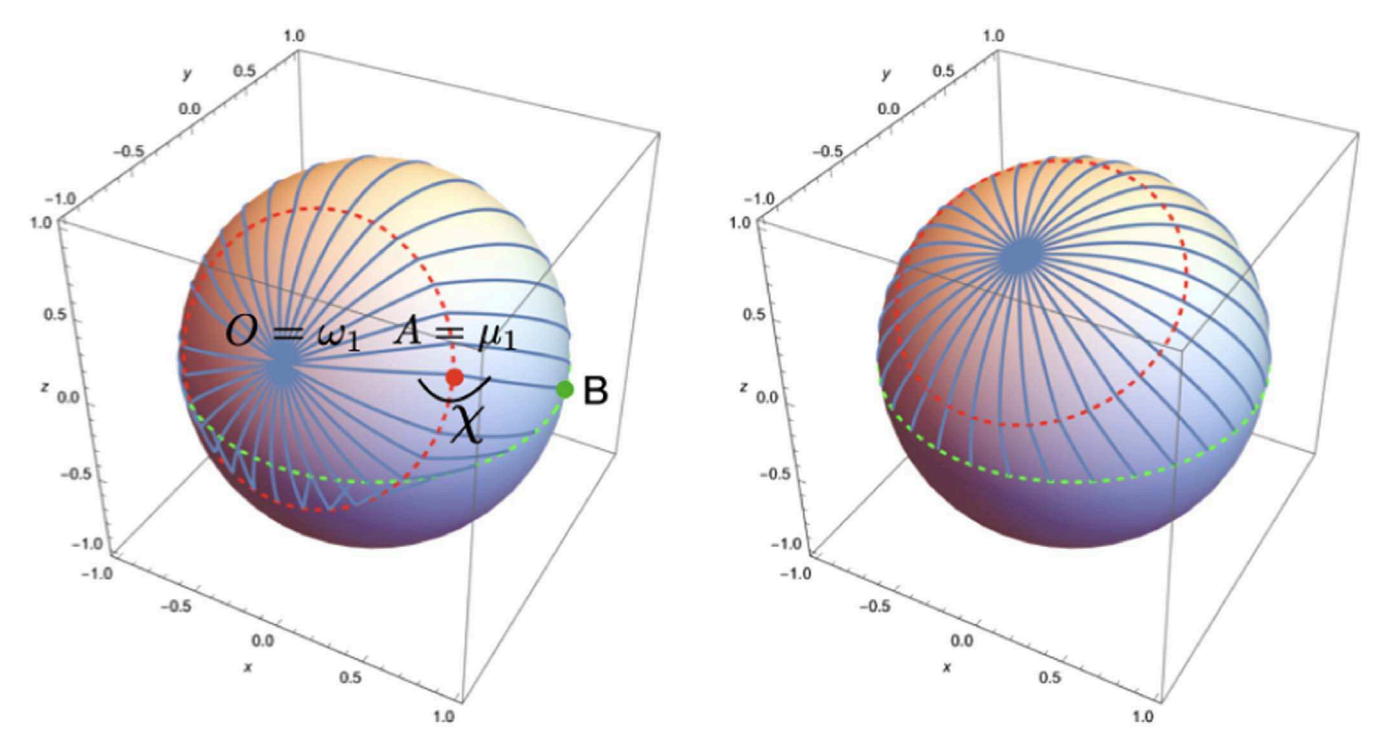


Figure 18. Example of twisting if/when the point A crosses the equator. The sphere represents a space of the directions of the magnetic field. The red dashed circle is the trajectory of the direction of the magnetic field at point A (direction of magnetic moment of 1); it rotates with the angular frequency  $\omega_A = \omega_1$  around point O, the direction of the spin of the first star. For both plots,  $\omega_1 = \Omega$ : one spin per one full orbital rotation. Left panel inclination  $\theta_A = \pi/3$ , right panel  $\theta_A = \pi/6$  (these are the angles between orbital momentum  $\vec{\Omega}$  and the spin  $\vec{\omega}_1$ . Radius of the circle  $\theta_{A,c} = \pi/4$  (this is the angle between the spin  $\vec{\omega}_1$  and the magnetic field  $\vec{\mu}_1$ ). Notice how arcs cross over in the lower part in the left panel, when point A is below the equator. To trace the twist, we follow the value  $\chi$  of the angle  $\angle OAB$  in Figure 19.

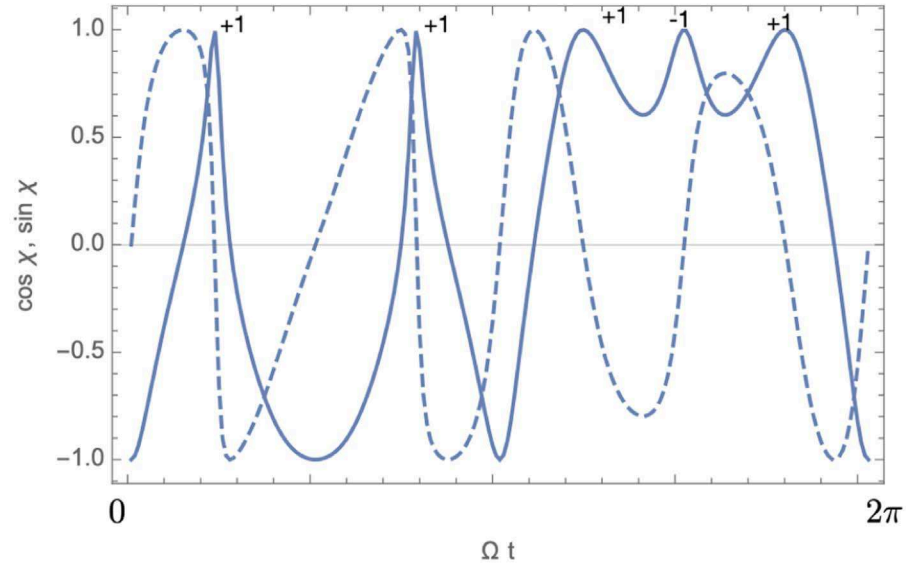


Figure 19. Counting the twist. Plotted is the angle  $\chi$ , spin of A, magnetic moment of A, direction to B,  $(\cos \chi, \sin \sin \chi, \sin \chi)$  dashed line). One rotation is added when  $\cos \chi = 1$  and  $\sin \chi$  changes from positive to negative; one rotation is subtracted when  $\sin \chi$  changes from negative to positive. In this example,  $\omega_A = 5\Omega$ ,  $\theta_A = \pi/3$  and  $\theta_{A,c} = \pi/4$ .

$$\begin{split} &-\omega_1\operatorname{sign}\vec{\omega}_1\cdot\vec{\mu}_2+\omega_2\operatorname{sign}\vec{\omega}_2\cdot\vec{\mu}_2\\ &+\Omega\left(\operatorname{sign}\vec{\Omega}\cdot\vec{\mu}_1-\operatorname{sign}\vec{\Omega}\cdot\vec{\mu}_2\right). \end{split} \tag{6}$$

The above holds so long as  $\alpha_i+\beta_i<\frac{\pi}{2}$  or after  $\alpha_i-\beta_i>\frac{\pi}{2}$  for i=1,2. Otherwise the circle on the direction sphere that  $\vec{\mu}_i$  traces out dips in the other hemisphere. What fraction of this

circle is in the other hemisphere? In other words, how long is the arc between the two points O and O' (see Figure 17) at which  $\vec{\mu}_1$  passes the equator?

Let  $\delta_1 = \frac{\pi}{2} - \alpha_1$  be the latitude of  $\vec{\omega}_1$ . Then from the spherical triangle formed by  $\vec{\omega}_1$ , O, and the equator midpoint M between O and O' we have

$$\cos \beta_1 = \cos a \cos \delta_1, \tag{7}$$

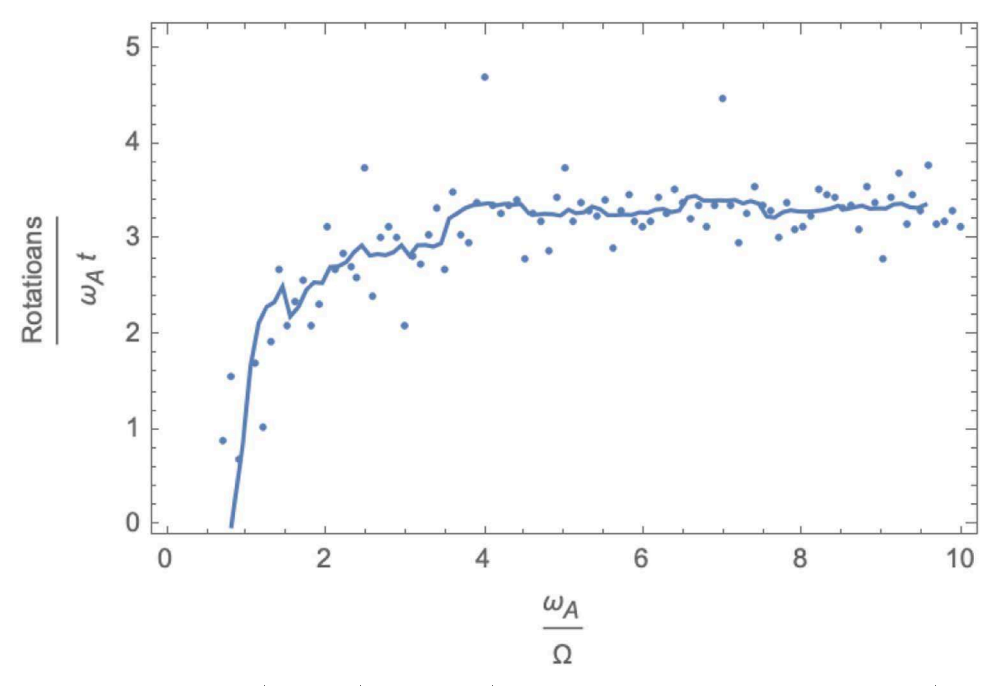


Figure 20. Rotations per unit time as a function of  $\omega_A/\Omega$ ,  $\theta_A=\pi/3$  and  $\theta_{A,c}=\pi/4$ ; the solid line is the running average. At large  $\omega_A/\Omega\geqslant 1$ , a finite limit is reached. Both the average curve and the variations carry information about parameters of the system.

$$\sin A = \frac{\sin a}{\sin \beta_1}.\tag{8}$$

Thus  $\sin A = \frac{\sqrt{\sin^2 \alpha_1 - \cos^2 \beta_1}}{\sin \alpha_1 \sin \beta_1}$ , and the fraction of the  $\vec{\mu}_1$  circle that is in the opposite hemisphere is

$$f(\alpha, \beta) = \begin{cases} \frac{2A}{2\pi} = \frac{1}{\pi} \arcsin \frac{\sqrt{\sin^2 \alpha - \cos^2 \beta}}{\sin \alpha \sin \beta} & \text{for } \frac{\pi}{2} - \beta < \alpha < \frac{\pi}{2} + \beta \\ 0 & \text{otherwise.} \end{cases}$$
(9)

Assuming for a moment that the rotation frequencies are much higher than the orbital frequency:  $\omega_1$ ,  $\omega_2 \gg \Omega$ , the average twisting rate  $\mathcal R$  is

$$\mathcal{R} = -(1 - 2f_1)\omega_1 \operatorname{sign}(\vec{\omega}_1 \cdot \vec{\mu}_1)$$

$$+ \Omega \operatorname{sign}(\vec{\Omega} \cdot \vec{\omega}_1) \operatorname{sign}(\vec{\mu}_1 \cdot \vec{\omega}_1)$$

$$+ (1 - 2f_2)\omega_2 \operatorname{sign}(\vec{\omega}_2 \cdot \vec{\mu}_2)$$

$$- \Omega \operatorname{sign}(\vec{\Omega} \cdot \vec{\omega}_2) \operatorname{sign}(\vec{\mu}_2 \cdot \vec{\omega}_2).$$
(10)

Here  $f_j = f(\alpha_j, \beta_j)$  given by Equation (9) with  $\alpha_j$  being the angle between  $\vec{\Omega}$  and  $\vec{\omega}_j$  and  $\beta_j$  angle between  $\vec{\omega}_j$  and  $\vec{\mu}_j$ .

This provides the average rate of winding of the magnetosphere for the general relative orientation of spins and orbital angular velocity. The averaging used applies whenever  $\omega_1$ ,  $\omega_2\gg\Omega$ . Figure 20 illustrates the time average converging to  $\mathcal{R}$ . Whenever the spins and angles are such that this rate  $\mathcal{R}$  is low, a slow winding of the magnetosphere is possible on average over time. This does not imply, however, that these configurations allow for gradual storage of energy in the magnetosphere, since the critical winding might/is likely to be breached in the interim. With this in mind, we focus on identifying other possible resonances.

#### 4.8. Importance of the Phase

We can have multiple non-winding resonances besides the 2:1 resonance; but their appearance depends on the phase. Thus, in a given system, one can observe several different resonances. These higher resonances, however, are much less stable.

Consider a snapshot with  $\omega_1$ ,  $\hat{R} = M$ , and  $\vec{\mu}_1$  aligned lying on a spherical radius of the blue disk in Figure 17. If, in the near future,  $\hat{R}$  reaches point O before  $\vec{\mu}_1$  does, then it also implies that, in the recent past,  $\vec{\mu}_1$  passed through point O' before  $\hat{R}$  did. In other words, the motion of  $\vec{\mu}_1$  over the arch O'O canceled the effect of  $\hat{R}$  traversing the equator (i.e.  $\vec{\mu}_1$  made one clockwise rotation around  $\hat{R}$ ). This is illustrated in the left-hand panel of Figure 18.

The necessary condition for such occurrence is  $\frac{a}{\Omega} < \frac{A}{\omega}$ , which translates to

$$\omega \arccos \frac{\cos \beta}{\sin \alpha} < \Omega \arcsin \frac{\sqrt{\sin^2 \alpha - \cos^2 \beta}}{\sin \alpha \sin \beta}.$$
 (11)

If the above snapshot occurs and the ration of the two frequencies is rational, the above snapshot will recur with regularity. E.g., if  $\frac{\omega_1}{\Omega}=\frac{2}{3}$ , then every two orbital periods  $\vec{\omega}_1$ ,  $\hat{R}$ , and  $\vec{\mu}_1$  are aligned again and the orbital winding effect is compensated by the above maneuver. Therefore, the effective magnetic tube winding rate is  $\omega_1-\Omega(1-\frac{1}{3})$ , which vanishes. In particular, if it so happens that  $\vec{\mu}_2$  is engaged in a similar resonant configuration, then the total winding rate is zero. To summarize, we have another resonant configuration

$$\omega_1 = \omega_2 = \frac{2}{3}\Omega, \quad \omega_1 + \omega_2 = \frac{4}{3}\Omega. \tag{12}$$

In contrast to 2:1 resonance, which was very stable with respect to changes of angles, phases, and frequencies, this 4:3 resonance is sensitive not only to angles and frequencies, but even to the phase, i.e., to the particular momentary (approximate) alignment.

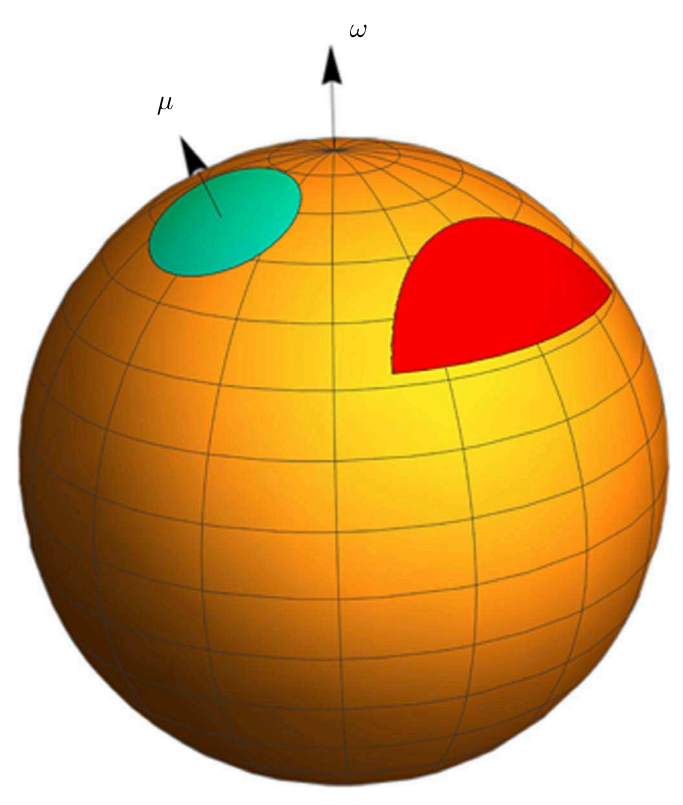


**Figure 21.** The magnetic cap, centered around  $\hat{\mu}$  in cyan and the resonant region in red for  $\lambda = \frac{\pi}{3}$ . A priori, the magnetic cap can be positioned anywhere on the sphere of directions. It is the overlap of the magnetic sphere and the resonant region that determines the part of the magnetosphere involved in the 4:3 resonance.

Nevertheless, during the binary evolution, such resonances can occur. Moreover, there are many other possible resonances. If they are observed, they can provide detailed information about the individual spins, their orientations, and about the orbital frequency.

Let us estimate the local region of magnetosphere that can contribute to the 4:3 resonance. The  $\hat{R}$  transit time (between O' and O) is  $T_R = \frac{2a}{\Omega}$ . The angular distance traveled by  $\hat{B}$  during this time is  $\omega T_R = \frac{\omega}{\Omega} 2a$ . The remaining angular span of the O'O arc (on the boundary of the blue spherical disk in Figure 17) is therefore  $2A - \frac{\omega}{\Omega} 2a$ . This is the arc of the  $\hat{B}$  points involved in the above described behavior leading to the 4:3 resonance. I.e., a point  $\hat{B}$  passes O' before  $\hat{R}$  does, and then  $\hat{B}$  passes O after  $\hat{R}$  does. Thus, for each value of  $\beta$ , there is an arc of angular size

$$2A - \frac{2\omega}{\Omega}a = 2\arcsin\frac{\sqrt{\sin^2 \alpha - \cos^2 \beta}}{\sin \alpha \sin \beta} - 2\frac{\omega}{\Omega}\arccos\frac{\cos \beta}{\sin \alpha}.$$
 (13)

The relevant solid angle formed by the magnetic line star surface directions involved in the resonance is

$$\int_{\frac{\pi}{2}-\alpha}^{\arccos\frac{\sin\alpha}{2}} (\sin\beta)(2A - 2\frac{\omega}{\Omega}a)d\beta. \tag{14}$$

The upper limit is reached when the equatorial arc O'O spans one-third of the equator, i.e.,  $2a<\frac{2\pi}{3}$ , implying  $\cos\beta<\frac{1}{2}\sin\alpha$ .

Now the fragility of this resonance can be illustrated in Figure 21. The resonant region, indicated in red, involves only those magnetic lines whose direction at the star surface lie in both the interacting magnetic polar cap (shown in cyan) and in the resonant (red) region. With our formulas above, one can estimate how likely it is that these two regions intersect at all and what the maximal overlap of these two regions can be.

#### 5. What Astrophysical Observational Effects We Expect: Precursor Flares in Merging Neutron Stars

Qualitatively, if only one star is magnetized, the corresponding slowly evolving powers are (Hansen & Lyutikov 2001; Lyutikov 2011)

$$L_{1M} \sim \frac{GB_{\rm NS}^2 M_{\rm NS} R_{\rm NS}^8}{cr^7}$$
  
= 3 × 10<sup>41</sup>(-t<sub>m</sub>)<sup>-7/4</sup> erg s<sup>-1</sup>. (15)

(Index 1*M* indicates here that the interaction is between a single magnetized neutron star and an unmagnetized one). The time to merger  $t_m$ 

$$-t_m = \frac{5}{256} \frac{c^5}{G^3} \frac{r^4}{M_1 M_2 (M_1 + M_2)}$$
 (16)

is measured in seconds in Equation (15).

Magnetospheric interaction of two *magnetized* neutron stars can generate larger luminosity: the interaction is between two magnetospheres, with effectively larger radius (Lyutikov 2019)

$$L_{2M} \sim \frac{B_{\rm NS}^2 G M_{\rm NS} R_{\rm NS}^6}{cr^5} = \frac{c^{21/4} B_{\rm NS}^2 R_{\rm NS}^6}{(-t)^{5/4} (G M_{\rm NS})^{11/4}}$$
$$= 6 \times 10^{42} (-t_m)^{-5/4} \text{ erg s}^{-1}. \tag{17}$$

(Index 2M indicates here that the interaction is between two magnetized neutron stars.) Thus  $L_2 \geqslant L_1$  dominates prior to merger.

Both powers (15)–(17) are not very large: they will be missed by high-energy observatories, but may be sufficiently bright if a large fraction is emitted in radio, producing a signal (Lyutikov 2019)

$$F_R \sim \eta_R \frac{L_2}{4\pi d^2 \nu} \approx 0.1 \text{ Jy } \eta_{R,-5} (-t)^{-5/4},$$
 (18)

where  $\eta_R$  is a fraction of the energy going into radio.

Topological resonance, especially the global one (1), allows two stars to establish a nearly permanent magnetic link. A slow change of the parameters would allow storage of magnetic energy within these configurations, and the subsequent release of the stored energy when the magnetic fields become too sheared/too twisted.

Equating neutron star beat-plus spins with the orbital frequency at separation *r* before the merger

$$\omega = \omega_1 + \omega_2 = 2\sqrt{\frac{G(M_1 + M_2)}{r^3}},$$
(19)

and using time to merger (16), the 2:1 resonance occurs at time

$$t_{1-2} = (-t_m) = 10^{-3} \frac{c^5 (M_1 + M_2)^{1/3}}{G^{5/3} M_1 M_2 \omega^{8/3}}$$
  
= 5 × 10<sup>5</sup> P<sub>s</sub><sup>8/3</sup> s, (20)

where  $P_s=2\pi/\omega$  is the sum-beat (addition) period of the NS spin's,  $M_1$  and  $M_2$  are masses of neutron stars (assumed to be equal to  $1.4M_{\odot}$ . Thus, the most interesting case is if one of the neutron stars is a recycled millisecond pulsar. For example, if  $P_s=10$  ms, then  $(-t_m)=2$  s. At that moment stars are separated by

$$r = (G(M_1 + M_2))^{1/3} \Omega^{-2/3} \approx 10^7 \text{cm},$$
 (21)

approximately 10 times the radius.

We can also estimate how flaring will evolve with time. At exact resonance, there is no shear, no flaring. As the orbit shrinks, the system gets out of the resonance, field lines are becoming twisted. Assuming that flares occur after a fixed twist angle  $\sim 1$ , time between flares can be expressed as

$$t_f = \frac{4P}{3\pi} \frac{t_{1-2}}{t - t_{1-2}}. (22)$$

Next, we need to estimate the amount of connected magnetic field lines. Vacuum dipoles provide a good first approximation to the magnetospheric structure. A simple case is that of antialigned magnetic moment, both orthogonal to the orbital plane. Let the two stars be located at  $\{x_{1,2} = \pm r/2, y_{1,2} = 0, z_{1,2} = 0\}$ . In the plane y = 0 (the plane that contains the vector connecting the stars and their magnetic moments), the total magnetic flux function is

$$\Psi_{\text{tot}} = \frac{(x - r/2)^2}{((x - r/2)^2 + z^2)^{3/2}} + \frac{(x + r/2)^2}{((x + r/2)^2 + z^2)^{3/2}}$$
 (23)

where  $\Psi$  is constant on each field line. The inner separatrix between regions (i) and (ii) are given by  $\Psi_{tot}=4/r$ , while outer by  $\Psi_{tot}=0$ . At large distances the outer separatrix are at 45 degrees.

For two neutron stars of radius  $R_{\rm NS}$  separated by distance r, the angular size of the patch of connected field lines can be estimated as

$$\theta_{\rm pc} \approx 2\sqrt{\frac{R_{\rm NS}}{r}}$$
 (24)

Thus, the energy in the connected magnetic field can be estimate as

$$E_{B,c} \approx \frac{B_{\rm NS}^2 R_{\rm NS}^4}{r}.$$
 (25)

Therefore, about one-tenth of the total magnetic energy can be released in a flare. For example, for merging neutron stars,

$$E_{B,c} \approx 0.08 \frac{B_{\rm NS}^2 R_{\rm NS}^4 \omega^{2/3}}{(GM_{\rm NS})^{1/3}} = 10^{41} B_{12}^2 P_{s,-2}^{-2/3} \,\text{erg},$$
 (26)

for a neutron star with a period  $P = 10^{-2}P_{s,-2}$  s. If reconnection occurs on light travel time over orbital separation, the expected power is

$$L_{B,c} = \frac{E_{B,c}}{r/c} = 10^{-1} \frac{B_{\rm NS}^2 c R_{\rm NS}^4 \omega^{4/3}}{(GM_{\rm NS})^{2/3}} = 3 \times 10^{44} B_{12}^2 P_{s,-2}^{-4/3} \,\text{erg s}^{-4/3}$$
(27)

This is a mild amount of energy/mild luminosity even for a fast-spinning ms neutron star. It still can be detected from  $\sim 100 \,\mathrm{Mpc}$  distances with all-sky high-energy monitors, and also can be seen in targeted observations (e.g., due to preliminary LISA

localization). Attempts to detect the precursor emission have been discussed by Callister et al. (2019) and Sachdev et al. (2020).

#### 6. Discussion

In this work, we consider the, topological structure of magnetically interacting binaries. We are particularly interested in configurations whose magnetospheres wind slowly—when the effects of spins and orbital motion (periodically) compensate each other. We point out that besides the very restricted cases of fully locked rotation and equal antiparallel spin in the orbital frame, there are other slow-winding configurations that can unwind locally (in a sense that a special set of magnetic tubes may wind slowly, while other magnetic tubes keep winding at high rate). The most interesting case is when the beat-plus frequency  $\omega_1 + \omega_2$  equals two times the orbital frequency. This globally non-winding configuration is achieved in a broad range of parameters (relative directions of spins, magnetic moments, and orbital angular momentum) that we identified.

There are no other globally unwinding configurations beside the tree cases mentioned above. But there can be specific magnetic tubes (with slow winding) connecting the two stars that are slowly winding, while other fields are are getting twisted. Whenever the fraction of such tubes is significant, one might expect gradual energy transfer from rotational to magnetic energy and its eventual release.

Our main mathematical perspective is viewing a magnetic tube as a line in the space  $\mathbb F$  of unit tangent circles to the two-sphere of directions. This makes apparent that the bifurcation point corresponds to one of the magnetic moments being (nearly) aligned with the binary separation vector:  $\vec{\mu}_1$  or  $\vec{\mu}_2 \| \mathbf{R}$ . The tube winding is due to 1) the spins twisting its two ends and 2) the orbital motion contributing one full twist to each half as  $\hat{R}$  orbits around  $\hat{\mu}_j$  in the sphere of directions. The latter effect originates in the topology of  $\mathbb F$ , which is a degree 2 Hopf fibration. It is this fact that ensures persistence and relative stability of the 2:1 resonance.

The main predicted phenomena for the case of merging neutron stars are the precursor flares, which can occur just few seconds before the main gravitational wave event (Hansen & Lyutikov 2001; Lyutikov 2019). The flare luminosity can be higher than the slowly varying persistent one; it is also easier to detect flaring events.

Curiously, since magnetic unwinding for other (not 2:1) resonances depends on phase, it may not occur every orbit, but with some periodicity. Analyzing the periodicity may constrain the absolute values of the spins. Generally, unwinding 2:1 resonance is very stable. Yet if higher order resonances are observed, a lot of detailed information may be inferred. Higher order resonances may have similar power to the basic one (Figure 21).

A few further modifications are planned. Elliptical orbits will add another complication: non-constant rotation of vector  $\mathbf{R}/$  point  $\mathbf{B}$ , which would rotate with changing Keplerian angular velocity. Our results, however, are essentially topological and thus should not be sensitive to such modifications.

Our perspective also calls for refinements, one can use it to obtain the rate of magnetic tube slow winding (without the averaging) and the rate at which the resulting energy is released (whenever the magnetic tube winding exceeds some critical value). One can also estimate the dependence of the resulting

energy release on the spin and orbital rotation parameters as well as its time signatures. All this is left for future exploration.

In application to exoplanet-star magnetic interactions, few comments are due. First, magnetic coupling between magnetospheres can occur only within the Alfvén radius of the parent star ( $\sim 10 R_{\odot}$  for the Sun). Tidal effects are likely to bring the system into corotation (Hut 1981, though more complicated dynamics like tidal spin-ups is also been considered (Tejada Arevalo et al. 2021)). For z-aligned spins this would make the magnetospheric structure in the rotating frame been static. On the other hand, there are evidence of cases of high obliquity, when the orbit of the star is highly inclined with respect to stellar spin (see Winn & Fabrycky 2015, for review). What is still required is alignment of at least one spin with the orbital angular momentum. Finally, there are indeed observations of the magnetospheric interactions of planet-modulated chromospheric and radio emission (Cauley et al. 2019; Vedantham et al. 2020; Turner et al. 2021).

The work of ML is supported by NASA grants 80NSSC17K0757 and 80NSSC20K0910, NSF grants 1903332 and 1908590. The work of SCh is supported by the Charles Simonyi Endowment at the Institute for Advanced Study.

We would like to thank Brad Hansen and Matt Shultz for discussions.

#### Data availability

The data underlying this article will be shared on reasonable request to the corresponding.

#### ORCID iDs

Sergey A. Cherkis https://orcid.org/0000-0002-0785-0126

Maxim Lyutikov https://orcid.org/0000-0001-6436-8304

#### References

```
Antoine, S. 2021, arXiv:2104.05968
Arnold, V. I. 1974, in Proc. Summer School in Differential Equations (Erevan:
   Armenian SSR A d Sci.)
Arnold, V. I. 1986, Selecta Math. Soviet, 5, 327
Bildsten, L., & Cutler, C. 1992, ApJ, 400, 175
Buckley, D. A. H., Meintjes, P. J., Potter, S. B., Marsh, T. R., &
  Gänsicke, B. T. 2017, NatAst, 1, 0029
Callister, T. A., et al. 2019, ApJL, 877, L39
Cauley, P. W., Shkolnik, E. L., Llama, J., & Lanza, A. F. 2019, NatAs, 3, 1128
Goldreich, P., & Julian, W. H. 1969, ApJ, 157, 869
Hansen, B. M. S., & Lyutikov, M. 2001, MNRAS, 322, 695
Hut, P. 1981, A&A, 99, 126
Lyutikov, M. 2011, PhRvD, 83, 124035
Lyutikov, M. 2019, MNRAS, 483, 2766
Moffatt, K., & Dormy, E. 2019, Self-Exciting Fluid Dynamos, Cambridge
  Texts in Applied Mathematics (Cambridge: Cambridge Univ. Press)
Most, E. R., & Philippov, A. A. 2020, ApJL, 893, L6
Palenzuela, C., Lehner, L., Ponce, M., Liebling, S. L., Anderson, M.,
  Neilsen, D., & Motl, P. 2013, PhRvL, 111, 061105
Radice, D., Perego, A., Hotokezaka, K., Fromm, S. A., Bernuzzi, S., &
  Roberts, L. F. 2018, ApJ, 869, 130
Rubenstein, E. P., & Schaefer, B. E. 2000, ApJ, 529, 1031
Sachdev, S., Magee, R., Hanna, C., et al. 2020, ApJL, 905, L25
Schaefer, B. E., King, J. R., & Deliyannis, C. P. 2000, ApJ, 529, 1026
Shultz, M., Wade, G. A., Alecian, E. & BinaMIcS Collaboration 2015,
     NRAS, 454, L1
Tejada Arevalo, R. A., Winn, J. N., & Anderson, K. R. 2021, ApJ, 919, 138
Turner, J. D., Zarka, P., Grießmeier, J.-M., et al. 2021, A&A, 645, A59
Vedantham, H. K., Callingham, J. R., Shimwell, T. W., et al. 2020, NatAs,
  4, 577
```

Warner, B. 1983, in Astrophysics and Space Science Library, 101, IAU Coll. 72: Cataclysmic Variables and Related Objects, ed. M. Livio & G. Shaviv (Dordrecht: Reidel Publishing), 155

Winn, J. N., & Fabrycky, D. C. 2015, ARA&A, 53, 409